Nature-inspired liquid crystalline systems and interaction of living organisms with liquid crystals

Won-Sik Kim*, Jun-Hyung Im*, Hyein Kim, Jin-Kang Choi, Yena Choi, and Young-Ki Kim†

Department of Chemical Engineering, Pohang University of Science and Technology (POSTECH), Pohang 37673, Republic of Korea

*These authors contributed equally to this work.

†Corresponding author. E-mail: ykkim@postech.ac.kr

Abstract

Biomaterials, which are substances interacting with biological systems, have been extensively explored to understand living organisms and obtain scientific inspiration (such as biomimetics). However, many aspects of biomaterials have yet to be fully understood. Because liquid crystalline phases are ubiquitously found in biomaterials (e.g., cholesterol, amphiphile, DNA, cellulose, bacteria), therefore, a wide range of research have made attempts to approach unresolved issues with the concept of liquid crystals (LCs). This review presents these studies that address the interactive correlation between biomaterials and LCs. Specifically, we first introduce intrinsic LC behavior of various biomaterials such as DNA, cellulose nanocrystals, and bacteria. Second, we address the dynamics of bacteria in LC media, with focus on how bacteria interact with LCs, and how dynamics of bacteria can be controlled by exploiting the characteristics of LCs. Lastly, we review how the strong correlation between LCs and biomaterials has been leveraged to design a new class of biosensors with additional functionalities (e.g., self-regulated drug release) that are not available in previous systems. Examples addressed in this review convey the message that the intersection between biomaterials and LCs offers deep insights into fundamental understanding of biomaterials, and provides resources for development of transformative technologies.

This article has been accepted for publication and undergone full peer review but has not been through the copyediting, typesetting, pagination and proofreading process, which may lead to differences between this version and the Version of Record. Please cite this article as doi: 10.1002/adma.202204275.

1. Introduction

At first, we introduce basic concepts of liquid crystals (LCs) to understand the contents of this review. Readers familiar with LCs may skip this section and move to next section.

Liquid crystals (LCs) are an intermediate phase of matter between liquid and crystal, having properties of both fluidity and long-range molecular ordering. The combination enables LCs to have extraordinary sensitivity to external stimuli, as well as anisotropic characteristics including birefringence, elasticity, and dielectric anisotropy. Therefore, LCs have been extensively explored as promising materials to design interactive systems that autonomously sense a programmed stimulus and alter the molecular orientation of LCs (defined by director **n**) on a macroscopic scale, thereby changing their physical/chemical characteristics. [1, 2] For instance, birefringence and stimuli responsiveness of LCs [3-6] have been used in information displays, sensors, [7-14] optofluidic, [15-17] and smart windows. [18, 19] Elasticity of LCs has been leveraged to control the force applied within LCs, which leads to the design of actuators, drug release systems, and controlled molecular/colloidal self-assembly. [7, 20, 21]

Generally, upon temperature changes, LCs show various states that are categorized according to orientational and positional ordering (so-called thermotropic LCs, Figure 1a). A nematic phase has only orientational ordering and a smectic phase has both orientational and positional ordering of LCs, while crystal and isotropic phases show perfect and no molecular ordering, respectively. [1, 2] In contrast, lyotropic LCs (LLCs) assume different states based on the concentration of composition in a solvent (Figure 1b). The states of LLCs are also dependent on temperature. [1, 2] For example, molecules of disodium cromoglycate (DSCG), the representative LLC, become stacked face-to-face and form elongated building blocks in a solvent as their concentration increases. This induced anisotropy causes orientational/positional ordering, and thus formation of LC phases. [22]

LCs can also assume a twisted structure, represented by cholesteric liquid crystals (CLCs) (Figure 1c). Quasi-layers induced by the chiral structure reflect a specific wavelength (λ_r) of light. The chiral pitch (p) can be modulated upon the introduction of stimuli, and thereby allow control of the reflected wavelength. This ability has been finding numerous applications including electronic paper, reflective displays, and spectral filters. [23, 24]

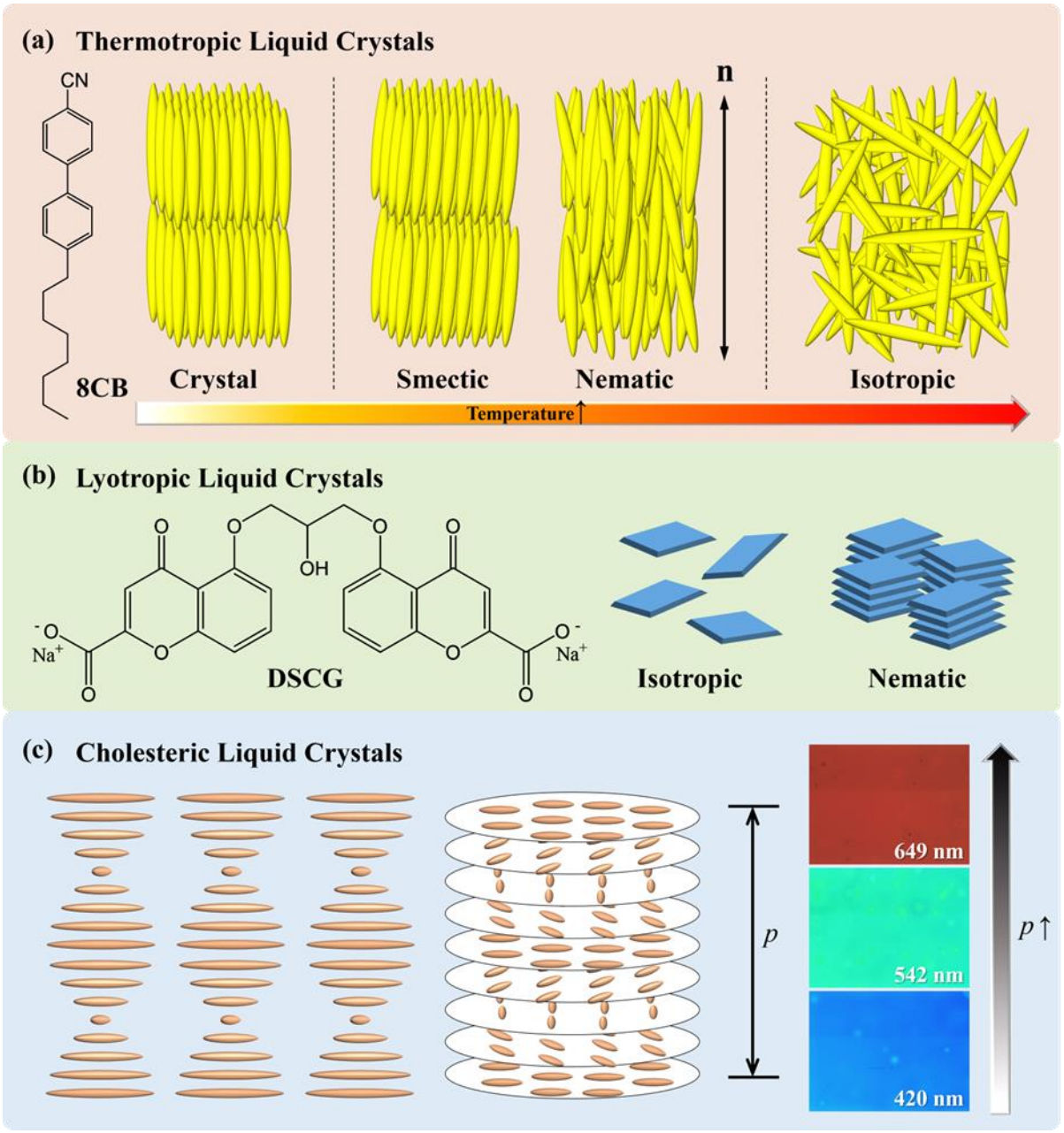

Figure 1. (a) Molecular structure of representative thermotropic LC, 4-cyano-4'-octylbiphenyl (8CB), and their phase behavior upon temperature changes. The existence of LC phases varies depending on the materials. For example, 4-cyano-4'-pentylbiphenyl (5CB) has only nematic LC phase. (b) Molecular structure of DSCG, representative LLCs. In water, the molecules stack on each other as their concentration increases, and form a LC phase. (c) Molecular configuration of CLCs with a chiral pitch *p* and corresponding micrographs showing different reflected colors with respect to *p*.

Type of topological defects and corresponding topological charges (m) found in LCs are shown in Figure 2a-d. In LCs, topological defects appear at which the orientational ordering of LCs cannot be defined. Therefore, LCs are "melted" in the defect core and their local orientational ordering is significantly diminished. [1, 2] Due to their thermodynamic stability and high energy density, the topological defects interact with each other (e.g., merging, splitting, collapsing) [2] and attract particles or molecules dispersed in LCs to replace the defect cores. [5, 6] The type and location of topological defects are precisely controllable, which is not possible in other phases of matter, so these characteristics have been applied in various fields to control, for example, molecular/colloidal self-assembly [17, 25] and colloidal motion. [26, 27] In addition, the topological defect plays an important role in determining the equilibrium configuration of LCs in confined systems (e.g., droplets) to satisfy both Poincaré and Gauss theorems. [2, 22, 28] When LCs are of the planar surface anchoring (**n** $\perp$ surface normal), LC droplets show the bipolar configuration with two point defects of m = +1 at poles (Figure 2e). Under the orientational transition from planar to homeotropic anchoring (**n** || surface normal) induced by, for example, self-assembly of amphiphilic molecules (e.g., surfactants) at the LC interface, however, the stable molecular configuration deviates from the bipolar structure (Figure 2e), first to axial (with a line defect (disclination) of m = +1/2, Figure 2f) then to preradial (with a point defect of m = +1 at the surface, Figure 2g), and then to radial configurations (with a point defect of m = +1 at the center of droplets, Figure 2h). [29]

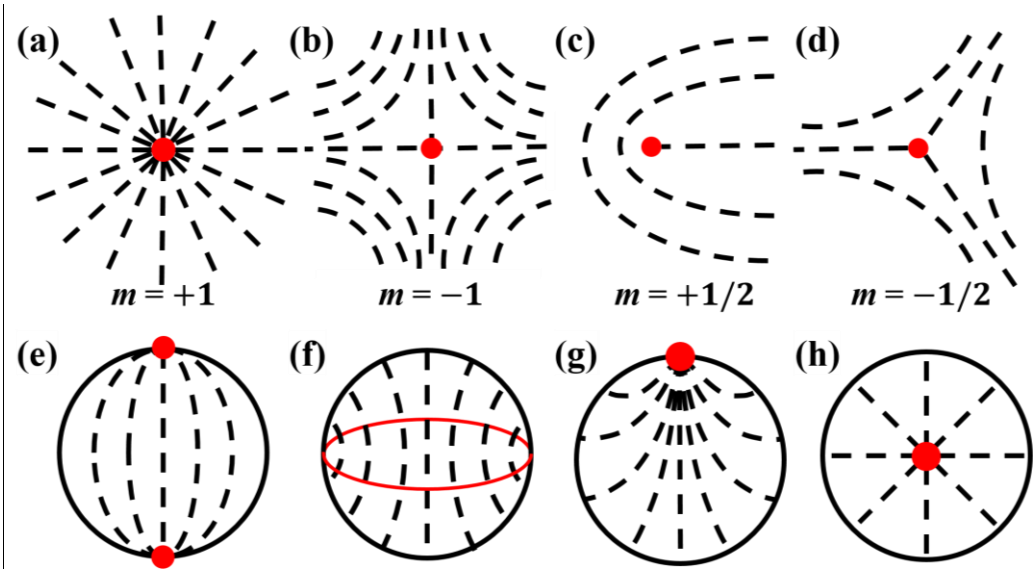

Figure 2. (a-d) Molecular orientation of LCs around topological defects of charge m = (a) +1, (b) -1, (c) +1/2, and (d) -1/2. (e-h) Molecular and defect configurations in LC droplets under

different surface anchoring conditions; (e) bipolar (two point defects of m = +1 at poles, planar anchoring), (f) axial (line defects (disclination) of m = +1/2, tilted anchoring), (g) preradial (a point defect of m = +1 at a pole, homeotropic anchoring), and (h) radial (a point defect of m = +1 at the center of droplet, homeotropic anchoring). Dotted black lines indicate director **n**. Red dots and solid line indicate topological defects.

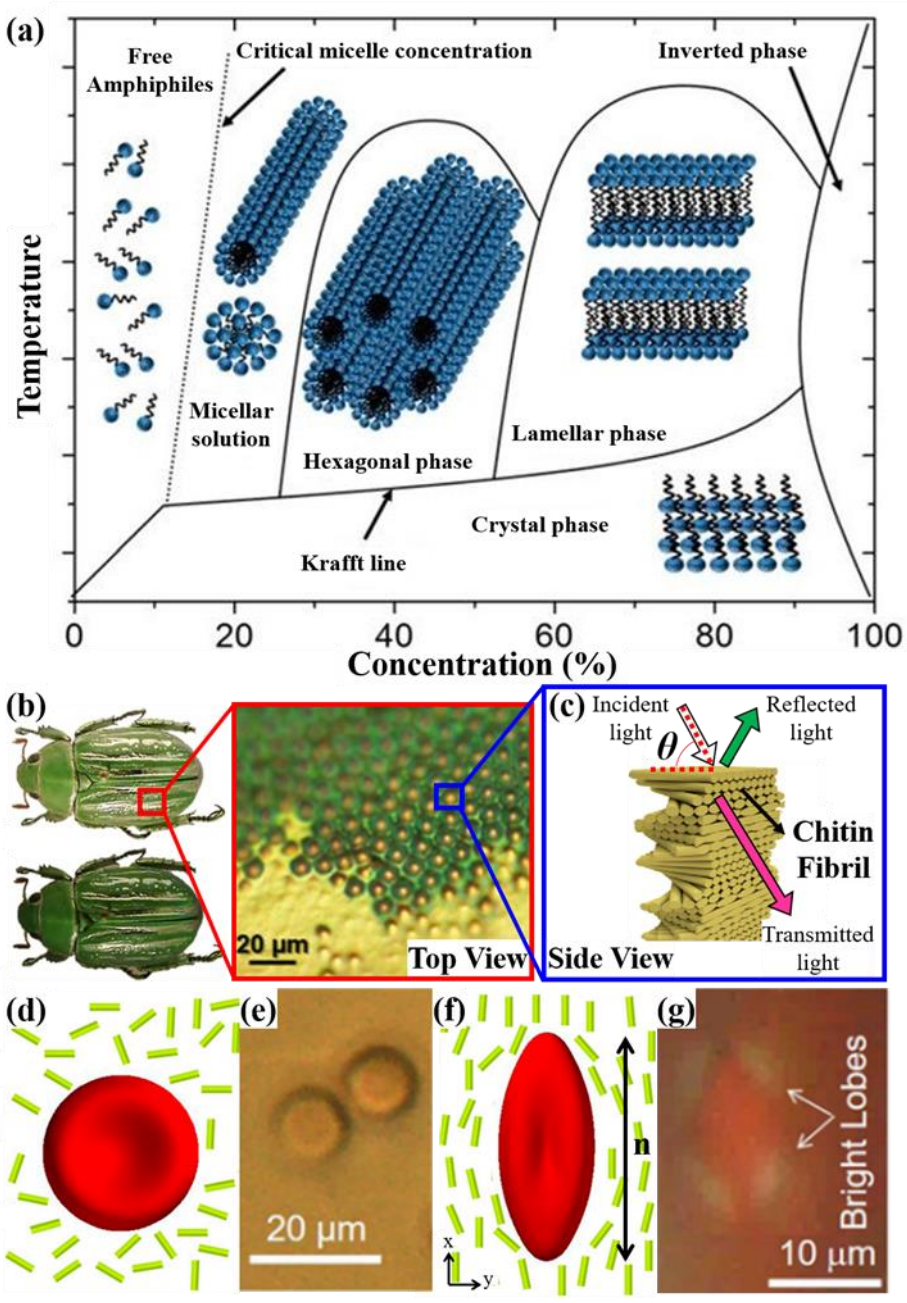

Figure 3. (a) Phase diagram of LLCs from amphiphilic molecules. (b) Structural colors of *Chrysina gloriosa* scarab beetle resulting from (c) the chiral organization of chitin molecules

(cholesteric phase). (d, f) Schematic illustrations and (e, g) corresponding micrographs of RBCs in (d, e) isotropic and (f, g) nematic DSCG solutions. (a) Reproduced under the terms of the CC-BY Creative Commons Attribution 4.0 International license (https://creativecommons.org/licenses/by/4.0/). [30] Copyright 2020, The Authors, published by MDPI. (b) Reproduced under the terms of the CC-BY-NC-ND Creative Commons Attribution 4.0 International license (https://creativecommons.org/licenses/by-nc-nd/4.0/). [32] Copyright 2014, The Authors, published by Elsevier, Reproduced with permission. [33] Copyright 2017, Elsevier. (c) Reproduced with permission. [31] Copyright 2012, American Association for the Advancement of Science. (d-g) Reproduced under the terms of the CC-BY Creative Commons Attribution 4.0 International license (https://creativecommons.org/licenses/by/4.0/). [35] Copyright 2020, The Authors, published by PNAS.

The introduced LC phases and characteristics are frequently observed in biomaterials. For instance, amphiphilic molecules found in many biological compounds (e.g., cholesterol derivatives, phospholipids, fatty acids) can itself form LLC phases in solvents. Above critical micelle concentration, amphiphiles self-assemble and form various anisotropic structures (e.g., elongated micelle, lamella). [30] Therefore, various LLC phases such as nematic, smectic, hexagonal, and lamellar can form in a certain concentration range (Figure 3a). The *Chrysina gloriosa* scarab beetle reflects colors with stripes of green and silver (Figure 3b) that are induced by the cholesteric structure of fibrils formed by chitin macromolecules (Figure 3c). [31-33] Therefore, by the Bragg effect, the chiral organization of chitin fibrils reflects a certain wavelength of incident light. The reflected wavelength of light is defined as $\lambda_r = n_{ave} \cdot p \cdot \sin\theta$ where n_{ave} is the average refractive index, and θ is the angle of incident light from the film surface (Figure 3c). [34]

Interactive relations between biomaterials and LCs facilitate the deep understanding of biomaterials. For example, several diseases can cause changes in the shape of red blood cells (RBCs), but these shape responses have been barely investigated. In recent works, Nayani *et al*. explore the shape transition of RBCs in LC media. [35] Specifically, RBCs dispersed in the isotropic phase of DSCG aqueous solution assume circular biconcave shapes (Figure 3d, e). As the solution forms a nematic phase upon increase in the concentration of DSCG, however, the induced elastic strain by LCs causes the RBCs to change shape to

elongated geometries along **n** (Figure 3f, g). The results demonstrate that the LC characteristics (e.g., elasticity and molecular ordering) of surrounding medium can regulate the shapes of soft colloids and provide insights into their mechanical properties. [35]

Media that have LC characteristics are ubiquitous (as will be introduced below), so research on coupling between biomaterials and LCs can provide insights into the characteristics and responses of biomaterials. In this review, therefore, we focus on the interaction between biomaterials and LCs, and on how these interactions have contributed to scientific knowledge and the design of smart materials. In Section 2, we explore LCs derived from biomaterials. We will review how DNA, cellulose, and bacterial colonies can show LC behavior, and how their LC characteristics have been utilized in a variety of fields. Section 3 reviews research on motile bacteria interacting with LCs. The effects of LCs' orientational ordering and elasticity on trajectories of bacteria will be described. Moreover, the active colloids driven by the controlled motion of bacteria will be covered. In Section 4, we illustrate the design of biosensors that exploit the interaction of LCs with biomaterials of DNA and bacteria.

2. Liquid Crystals from Biomaterials

2.1. LCs from DNA

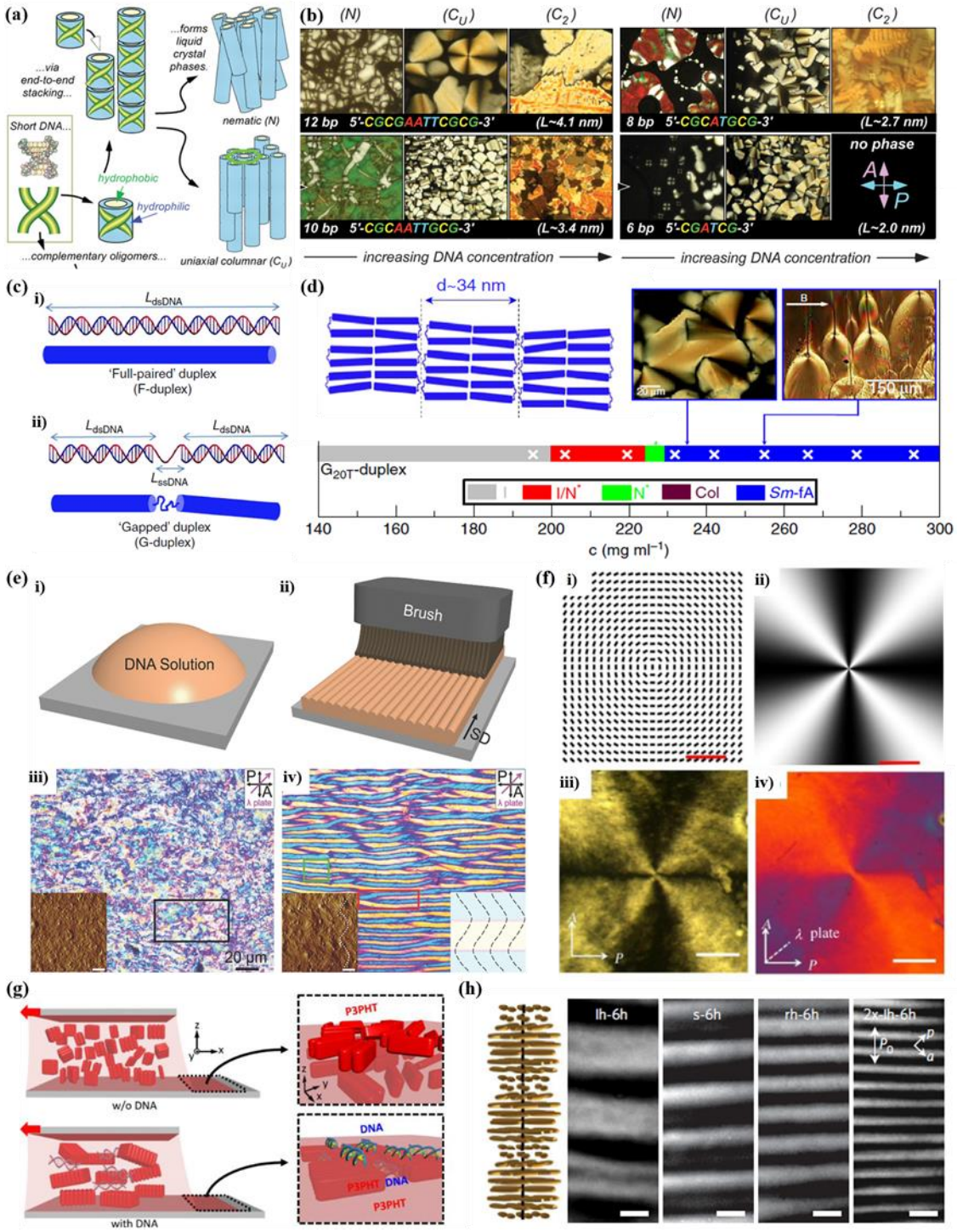

Figure 4. (a) Schematic illustration for formation of LC phases by end-to-end stacking of short DNA fragments. (b) Optical micrographs of various LC phases from short (6~12 base pair) DNA fragments. N, C_U, and C_2 indicate nematic, uniaxial columnar, and higher-ordered columnar phases, respectively. A and P represent the polarization of analyzer and polarizer, respectively. (c) Structures of 'Full-paired' DNA duplex and 'Gapped' duplex. 'Gapped' duplexes have a flexible single-strand chain between double-strand chains. (d) Phase diagram

of 'Gapped' duplex solution in terms of DNA concentration with molecular organization and corresponding micrographs in a 'Hidden' smectic phase. (e) i, ii) Schematic images and iii, iv) corresponding micrographs of DNA-based LC solution on a degenerate substrate i, iii) without and ii, iv) with shear stress applied by brushing. Micrographs are observed between crossed polarizers with λ-plate. (f) Photo-patterned i) director profile of DNA-based LC solution around a topological defect of m = +1 and corresponding micrographs from ii) simulation and iii, iv) experiments between crossed polarizers (iv with λ-plate). Scale bar, 50 μm. (g) Schematic illustrations of formation of unidirectional alignments of poly[3-(potassium-7-hexanoate)-thiophene-2,5-diyl] (P3PHT) in the liquid crystalline template of DNA: top, degenerate alignment of P3PHT; bottom, unidirectional alignment of P3PHT with DNA matrix. (h) Schematic and corresponding fingerprint textures of cholesteric phases from DNA filament solution. Scale bar, 20 μm. (a, b) Reproduced with permission. [53] Copyright 2007, American Association for the Advancement of Science. (c, d) Reproduced under the terms of the CC-BY Creative Commons Attribution 4.0 International license (https://creativecommons.org/licenses/by/4.0/license). [63] Copyright 2016, The Authors, published by Springer Nature. (e) Reproduced with permission. [69] Copyright 2016, WILEY-VCH. (f) Reproduced with permission. [71] Copyright 2020, American Physical Society. (g) Reproduced with permission. [78] Copyright 2020, American Chemical Society. (h) Reproduced with permission. [80] Copyright 2017, Springer Nature.

DNA has been theoretically and experimentally demonstrated to exhibit LC phases in aqueous solutions at sufficiently high concentration. [36] Onsager theory thermodynamically elucidating the effect of shape of colloidal particle predicts that the long and thin rod-like particle (L/D >> 1, L: length, D: diameter) undergoes entropy-driven isotropic-to-nematic phase transition to minimize excluded volume. [1, 2, 30, 37] Computational simulations show that the excluded volume effects of non-spherical hard-core or semi-flexible chain models can also cause nematic, smectic, and columnar phases for particular ranges of small L/D. [1, 2, 38-40] Integrating them, Bolhuis and Frenkel present a complete phase diagram of spherocylindrical particle from L/D = 0 to ∞ by computational simulation, which shows formation of nematic and smectic phases above the critical aspect ratio of L/D = 4.7 (corresponding to 28 base pairs (bp) of DNA), below which isotropic-to-LC phase transition is not expected due to insufficient entropic driving force. [41]

As expected by theoretical works, long DNA fragments from 150 to thousands of base pairs ($25 \leq L/D \leq 1000$, which is beyond the critical $L/D = 4.7$) have been experimentally shown to form LC phases in the aqueous-salt or aqueous-polymer solutions with DNA concentration of 100 ~ 200 mg/ml. [42-45] The DNA-based LC solutions are generally prepared by two methods: 1) direct dissolution of lyophilized DNA in a very small amount of buffer solution followed by addition of water and 2) ultrafiltration of DNA solutions via a semipermeable membrane that allows no passage of DNA fragments. [46-48] Specifically, in 1961, Robinson first observed a periodic dark-bright pattern in calf thymus DNA solution after drying it in a capillary. [49] The pattern, known as fingerprint texture, indicates the chiral nematic phase (cholesteric phase). Subsequent experimental results using X-ray diffraction, small-angle light scattering and other methods have confirmed the existence of various LC phases of DNA. [50-52]

Contrary to the theoretical model, however, ultrashort DNA oligomers from 6 to 20 bp (< critical number 28 bp) are also shown to form nematic and columnar phases (Figure 4a, b). [53] Once the complementary DNA oligomers combine into longer DNA duplexes (also known as DNA mesogens), their end-to-end adhesion from hydrophobicity of terminal end induces self-assembled linear aggregates, which have leading to enough anisotropy and rigidity to form a LC phase (Figure 4a). [53] This end-to-end adhesion is the distinctive feature of DNA mesogens, and also enables development of LC phases even by very short fragments < 6 bp. For instance, 4-bp DNA oligomer can achieve a LC phase by a "running bond" type of pairing. [54] The underlying mechanism is similar, but DNA oligomer hybridization occurs continuously in a single process over the whole region of oligomer, not only at the end region, leading to the formation of long linear chains. More recently, even nucleic acid monomers have been shown to form a LC phase. [55] Base-paired nucleic acid mononucleotide triphosphates are stacked by chromonic amphiphilicity, thus exhibiting columnar LC phase.

Upon increases in DNA concentration, isotropic phase of linear DNA fragment solution typically turns to a blue or pre-cholesteric phase, then to a cholesteric phase, then to a columnar hexagonal phase, and then to a crystalline (orthorhombic) phase. [36] The critical DNA concentration and phase behavior can be tuned by adjusting the structure of DNA fragment, ionic strength, and polymer concentration in the solution. [43] For instance, longer DNA fragments which have larger excluded volume encourage the formation of the LC

phase. Also, due to the polyelectrolyte nature of DNA from a negatively-charged phosphate group, the ionic strength of the solution strongly affects the phase behavior of LC. For instance, presence of metal cations can reduce the electrostatic repulsion between the phosphate groups of DNA fragments, thus inducing their condensation. [44, 56] Furthermore, hydrophilic neutral polymer (e.g., polyethylene glycol (PEG)) in the DNA solution can cause phase exclusion of DNA fragments (kwon as "Ψ-condensation"). [47, 57, 58] However, temperature of the DNA solution does not affect the critical concentration, confirming the entropic driven phase transition. [44]

Although the smectic phase of rod-like particles has been demonstrated theoretically [59] and experimentally [60], the smectic phase of DNA was not observed until recently. Livolant *et al*. show that the preference of 2D columnar formation of DNAs prevents development of the 1D smectic layer, but the mechanism is not understood. [61, 62] This 'hidden' smectic phase of DNA is finally realized by using 'Gapped' DNA duplex (G-duplex) in which single-stranded DNA (ssDNA) joins double-stranded DNA (dsDNA) regions, and thus increases molecular flexibility (Figure 4c). [63, 64] It is an interesting result because the increased flexibility suppresses formation of a smectic layer. [65] In this phenomenon, however, the end-to-end adhesion also has an important influence. In conventional (fully-paired) DNA duplexes, the hydrophobic end-to-end interaction causes non-uniform polydisperse DNA aggregates, which prevents formation of a uniform smectic layer. In the G-duplex, however, the flexibility imparted by the ssDNA connectors enables evolution of a folded structure that self-protects from the end-to-end attraction, and thus permits formation of a uniform smectic layer (Figure 4d).

The LC behavior of DNA has been exploited to not only understand its biological behavior, but also to design the desired orientation or structure of DNAs. To this end, methods that use shear stress, drying, and magnetic field had been reported. [66-68] Specifically, shear-induced flow by brushing is shown to generate zig-zag alignment of DNA arrays from degenerate alignments on a substrate (Figure 4e). [69] In addition, the presence of micro-posts on the substrate can help to control the shear-induced DNA alignment. [70] Photo-patterning can also be used to align DNAs (Figure 4f). [71] When a DNA solution is coated on a photo-alignment layer of azo-dye molecules that is exposed to linearly-polarized UV light, **n** of DNAs is found to be tangentially aligned perpendicular to the polarization of UV light. The results demonstrate that various DNA configurations can be programmed from

micrometer to millimeter length scale. Such a DNA matrix with predesigned orientations can be exploited as the alignment template for gold nanorods, [70] bacteria, [72] thermotropic LCs, [73, 74] and polymers. [75, 76] For instance, in organic optoelectronic devices (e.g., organic field effect transistors), the uniform alignment of organic polymer is required for better electrical performance, because disordered structure incurs defects like grain boundaries and reduces charge-carrier mobility. [77] As shown in Figure 4g, the unidirectionally aligned DNA matrix that results from their LC characteristics can be used as a template to achieve highly-ordered organic conducting polymer. [78]

DNA origami is a process that folds DNA to produce 2D or 3D nanostructures, and is another approach to modulate LC behavior of DNAs. [79] Siavashpouri *et al*. show the assembly of DNA origami filaments can assemble to induce the cholesteric phase showing fingerprint textures (Figure 4h). [80] They find the degree of twist along the filament's long axis to influence *p* of the induced cholesteric phase; smaller *p* from more twisted filaments. Furthermore, *p* can be tuned continuously by mixing two filaments with opposite chirality. The results demonstrate that the microscopic structure of DNA filaments can influence the macroscopic properties of LCs (e.g., chiral pitch of bulk cholesteric phase).

2.2. LCs from Cellulose

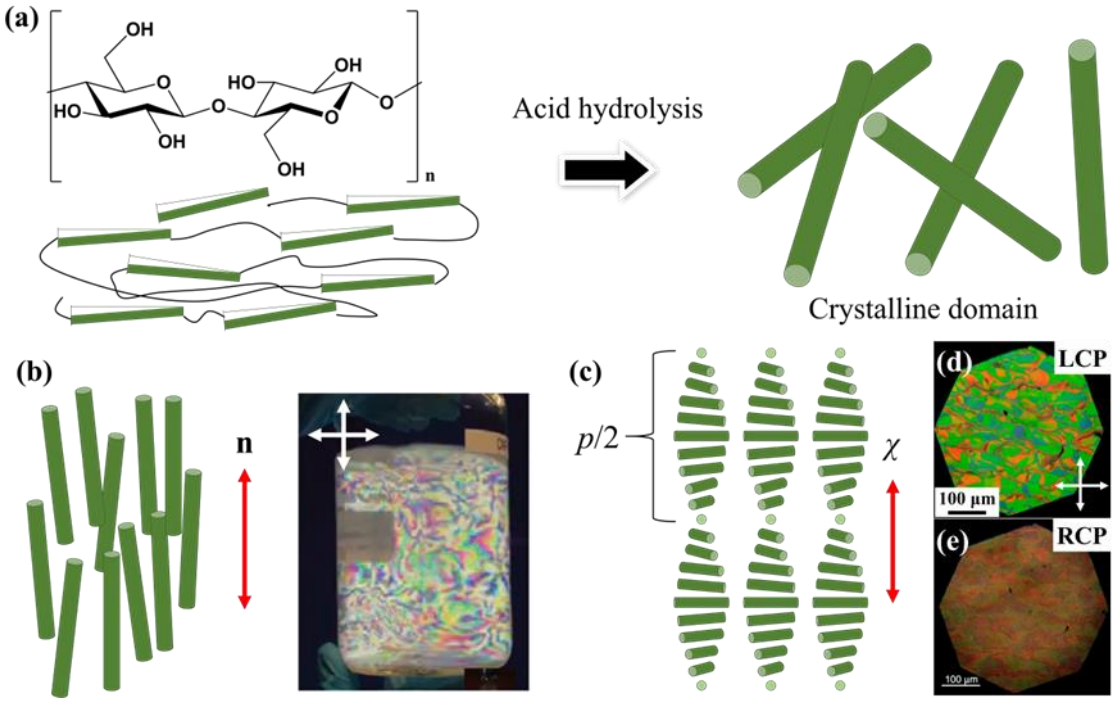

Figure 5. (a) Schematic illustrations of formation of crystalline domain of CNCs by acid hydrolysis. They exhibit an isotropic phase below Onsager's critical concentration *c* of CNCs in a solvent. (b) Schematic for molecular orientation of CNCs in a nematic phase and corresponding optical image between crossed polarizers. (c) Schematic for molecular orientation of CNCs in a cholesteric phase and (d, e) corresponding reflection micrographs between crossed polarizers under the incident lights of (d) left- and (e) right-handed circular polarizations. White arrows indicate the polarization of polarizer and analyzer. (a) Reproduced with permission. [34] Copyright 2020, Wiley-VCH. (b) Reproduced with permission. [82] Copyright 2020, Wiley-VCH. (d, e) Reproduced under the terms of the CC-BY Creative Commons Attribution 4.0 International license (https://creativecommons.org/licenses/by/4.0/). [83] Copyright 2014, The Authors, published by American Chemical Society.

Cellulose nanocrystals (CNCs) can be obtained from various cellulose resources such as trees, plants, bacteria, and fungi. [34, 48] When the cellulose comprised of β-(poly-1,4-D-glucose) is hydrolyzed by acid, only the crystalline domains of cellulose (rod-like CNCs) remain (Figure 5a). [34, 48, 81] The CNCs are generally hundreds of nanometers long (length *L*) and tens of nanometers wide (diameter *D*); the dimension depends on the sources and on the hydrolysis condition. [48] When rod-like CNCs are prepared as a suspension in water, they undergo the phase separation above the Onsager critical concentration ($c \approx 4/\xi_{\text{eff}}$, where ξ_{eff} is an effective *L*/*D* of nanocrystals) to minimize excluded volume. [37, 82] Consequently, depending on *L*/*D* and preparation condition, CNCs can assume a nematic or a cholesteric phase (Figure 5b, c). [34, 48, 82-85]

One intriguing feature of CNCs is their capability of spontaneous self-assembly into a left-handed helicoidal nanostructure where CNCs are twisted along the helical axis χ and thus form quasi-layers at intervals of $p/2$ (Figure 5c). [34, 48, 82] Therefore, the cholesteric CNC films reflect a certain wavelength of incident light in the same manner as photonic structures which can be observed in, for example, a jewel beetle (Figure 3c).

CNCs are abundant and renewable and can be used to precisely control the wavelength of reflected light, so they have been evaluated as promising photonic materials. [83-92] For instance, CNCs have been used to develop films that have asymmetric dichroism

[85] because spontaneous left-handed chirality of CNCs derived from their asymmetric carbons [48] enables selective reflection of light with left-handed circular polarization (LCP, Figure 5d), whereas a significantly low reflection of right-handed circular polarization (RCP, Figure 5e). [83] In other optical applications, however, this advantage is also a drawback because only half of the light is used. To solve this problem, De La Cruz *et al*. recently report cholesteric CNC films that can reflect both LCP and RCP sandwiching a LC retarder between two CNC films. [89]

Evaporation-induced self-assembly (EISA) has been used to prepare cholesteric CNC films from micrometer to meter scale. [93] Control of evaporation rate and circumstances can regulate initial p and χ (and thus λ_r) of resulting CNC films. [83, 84, 86, 87] For instance, the diamagnetic susceptibility of CNCs can be exploited to control the orientation of χ by applying a magnetic field (***H***) during EISA. [84] The tuned χ of CNCs is demonstrated by the color gradients of resulting CNC films from the junction of opposite magnets (Figure 6a). Specifically, SEM micrographs demonstrate that in the absence of ***H***, the CNC films form with a tilted helical axis, which is indicative of inhomogeneous χ and λ_r (Figure 6b left). Application of ***H*** perpendicular to the surface of CNC films induces development of homogeneous distribution of χ (tilted angle ~ 0°) parallel to the direction of ***H*** (Figure 6b right).

Recent studies have achieved reconfigurable CNC films that report various external stimuli by a color transition arising from changes in p. [88, 90-92] For example, CNC films can be designed to respond to relative humidity (RH) by doping PEG. [88] When an aqueous mixture of CNCs and PEG is dried, iridescent films of cholesteric CNCs form (Figure 6c). The PEG intercalated between CNCs determines the initial p. CNCs are hydrophobic and PEG can be swollen by water, so p can be manipulated upon changes in RH (Figure 6d). λ_r red-shifts as RH increases, indicating that swelling of PEG increases the p of CNC/PEG composite films. CNCs can be also used to report mechanical stress by changing color depending on the amount of tension applied (Figure 6e). [90] To obtain resistance to tensile strength, cholesteric CNC films are mixed with an elastomer that is composed of ethyl acrylate and 2-hydroxyethyl acrylate. The resulting film exhibits vivid yellow color between crossed polarizers and the color changes to green when the CNC/elastomer composite film is stretched in the direction of the tensile strain. This color transition is caused by increase in optical retardation of the film because the mechanical stretching unwinds the twisted ordering

of CNCs (insets in Figure 6e). These studies demonstrate that CNCs can be used in design of smart materials that can detect and self-report various stimuli.

LC behavior of CNCs has been also utilized to control self-assembly of guest materials. [85, 94-97] When cholesteric CNC droplets (Figure 6f) doped with monomers are photopolymerized and then the CNCs are removed, the guided ordering of monomers by CNCs is observed to induce formation of polymeric microspheres that have internal chiral structures (Figure 6g). If the CNC solution of cholesteric phase is confined by two substrates with a homeotropic anchoring it shows the fingerprint texture (indication of cholesteric phase, Figure 6h). [96] Bright regions caused by high retardation imply tangential alignment of CNCs with respect to substrates, whereas extinction lines indicate vertical orientation of CNCs. When gold nanorods (GNRs) are doped into the CNC films, their alignments are mediated by the chiral organization of CNCs as demonstrated by two-photon luminescence (TPL). The intensity of TPL is maximized when the polarization of excitation light ($\mathbf{P}_{ex}$) is consistent with the long axis of GNRs (Figure 6i), indicating that the GNRs are aligned parallel to **n** of CNCs (inset in Figure 6h). We also note that individual CNCs are recently being used as templates for carbon dots to generate dissymmetric emission because CNCs are mainly comprised of carbon and have left-handed chirality. [98]

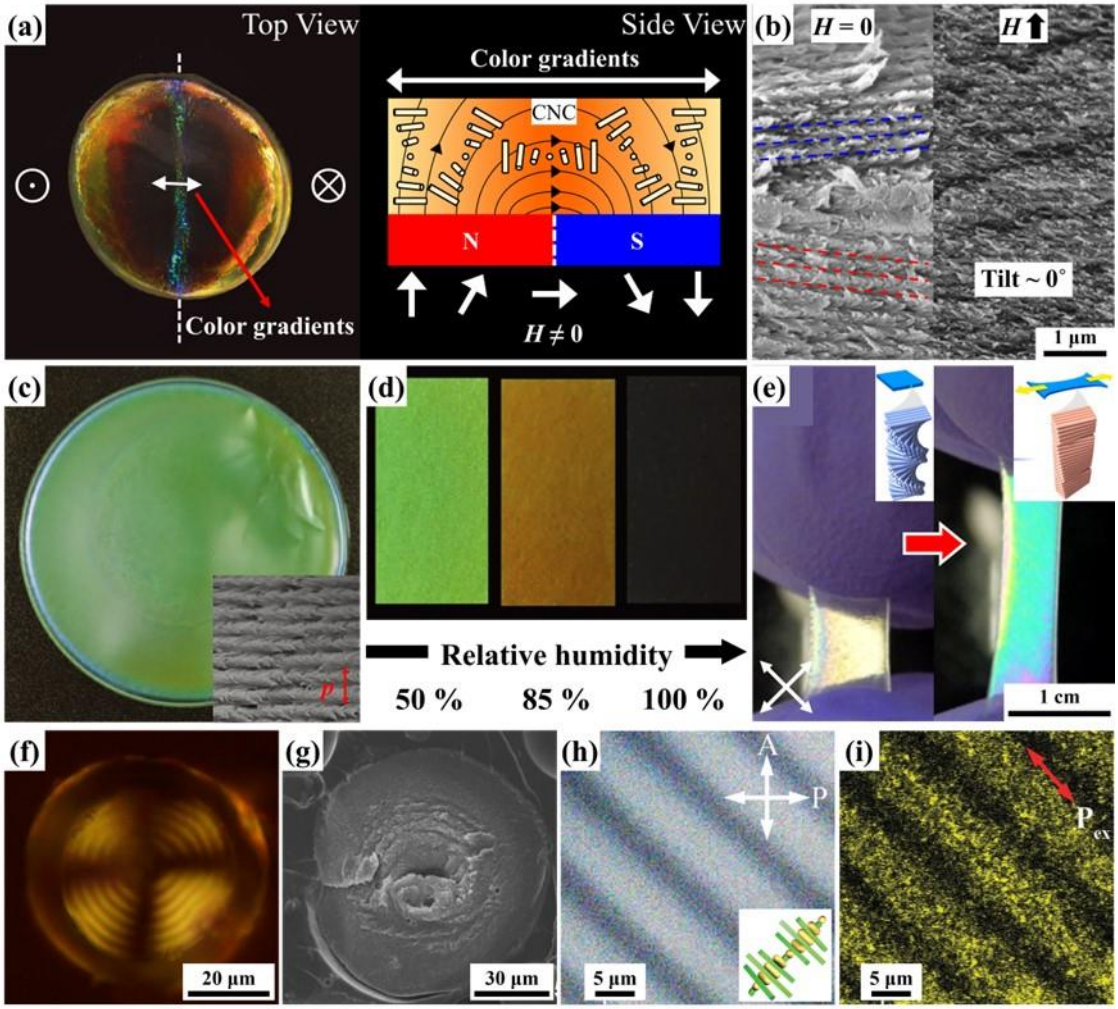

Figure 6. (a) Photograph (top view) and schematic illustration (side view) of cholesteric CNC film under magnetic fields. White dashed line indicates junction of two opposite magnets. Color gradients of the CNC film are attributed to field-induced reconfiguration of chiral structure. (b) Corresponding cross-sectional SEM images of CNC films without (left) and with (right) magnetic fields. Red and blue dashed lines indicate CNC layers. (c) Photograph of humidity-responsive CNC/PEG film and a cross-sectional SEM image. (d) Optical reporting of the CNC/PEG films with respect to relative humidity. (e) Photographs of mechanical-responsive CNC/elastomer films between crossed polarizers when unstretched (left) and stretched (right). Insets show the corresponding schematic illustrations of the internal ordering of CNCs. (f) Micrograph and (g) cross-sectional SEM image of polymeric microsphere templated by CNC droplet. (h) Micrograph of CNC film doped with gold nanorods (GNRs) confined between two substrates with homeotropic surface anchoring. Inset shows the organization of GNRs templated by chiral orientation of CNCs. The helical axis χ of CNC film is aligned 45° to polarizers. (i) Corresponding two-photon luminescence (TPL)

image under $\mathbf{P_{ex}} \perp \chi$. (a, b) Reproduced under the terms of the CC-BY Creative Commons Attribution 4.0 International license (https://creativecommons.org/licenses/by/4.0/). [84] Copyright 2017, The Authors, published by Wiley-VCH. (c, d) Reproduced with permission. [88] Copyright 2017, Wiley-VCH. (e) Reproduced under the terms of the CC-BY Creative Commons Attribution 4.0 International license (https://creativecommons.org/licenses/by/4.0/). [90] Copyright 2019, The Authors, published by Spring Nature. (f, g) Reproduced with permission. [97] Copyright 2016, Wiley-VCH. (h, i) Reproduced with permission. [96] Copyright 2014, Wiley-VCH.

2.3. LCs from Bacteria

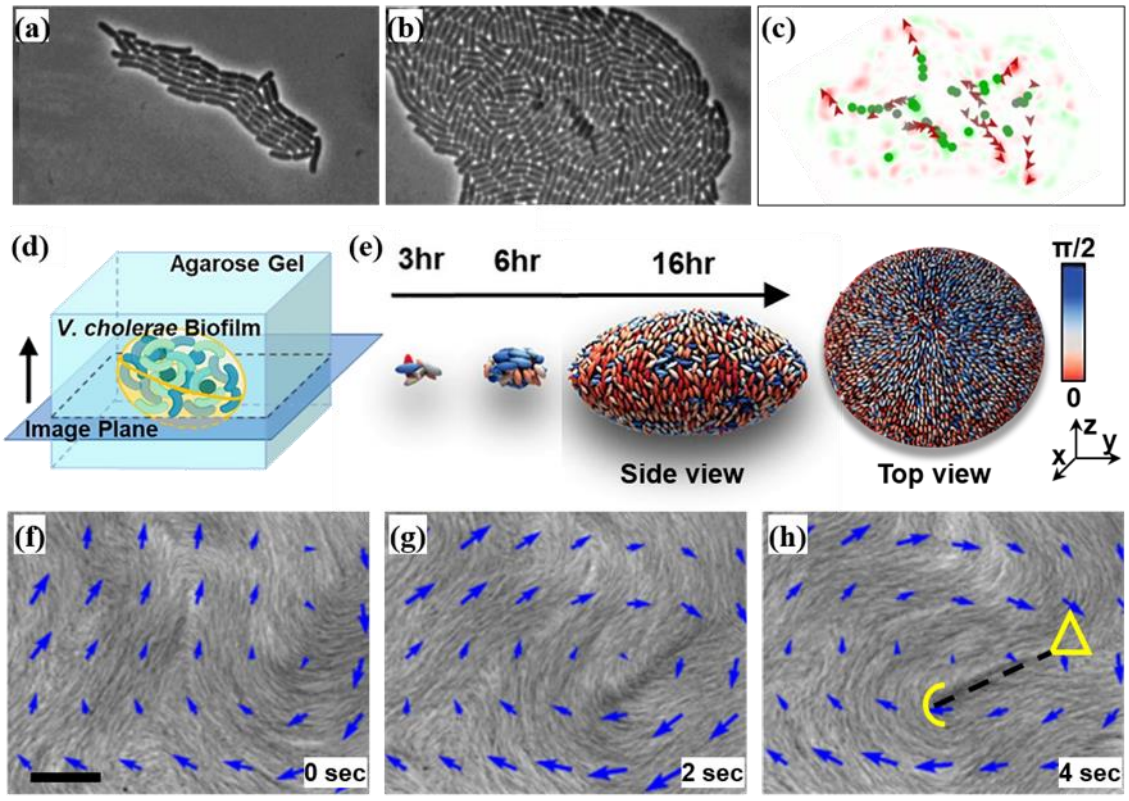

Figure 7. (a, b) Sequential micrographs of a growing bacterial colony exhibiting LC behavior and (c) measured trajectory of topological defects within the colony. Red arrows and green circles correspond to the topological defects of $m = +1/2$ and $-1/2$ defects, respectively. (d) Schematic illustration and (e) sequential reconstructed images of *Vibrio cholerae* biofilm growing in agarose gels. (f-h) Sequential micrographs of nematic phase of DSCG solution containing motile bacteria. Blue arrows indicate local flow velocity and direction. Yellow

triangle and semicircle indicate the topological defects of $m = -1/2$ and $+1/2$, respectively. Scale bar, 30 μm. (a-c) Reproduced with permission. [102] Copyright 2018, Springer Nature. (d, e) Reproduced under the terms of the CC-BY Creative Commons Attribution 4.0 International license (https://creativecommons.org/licenses/by/4.0/). [100] Copyright 2021, The Authors, published by PNAS. (f-h) Reproduced under the terms of the CC-BY Creative Commons Attribution 4.0 International license (https://creativecommons.org/licenses/by/4.0/). [103] Copyright 2014, The Authors, published by PNAS.

Biofilms are communities of microorganisms (e.g., bacteria) adhered to surfaces. [99] Typically, biofilms are observed in soft and confined environments, such as food matrices and host tissues, which are essential for cell reproduction. [100] Therefore, understanding of how a single bacterium becomes a colony of many thousands of cells is important in biomedicine and food safety. [101] This process in molecular and genetic aspects has been extensively explored, but the underlying mechanisms are still poorly understood. Recently, Dell'Arciprete *et al.* analyze the growth of micro-colonies of rod-shaped bacteria (*Escherichia coli*) in a single layer (quasi-2D) and find them to show LC behavior (named 'living anisotropic fluid'). [102] Specifically, as cells grow, their colony initially expands along the long axis of bacteria (Figure 7a). Later, this one-dimensional orientation breaks down, to yield a pattern of nematic domains with creation, migration, and merging of topological defects of $m = \pm 1/2$ (Figure 7b, c).

Subsequently, Zhang *et al.* investigate the growth of biofilms in three-dimensional environments (Figure 7d) and demonstrate that the relative stiffness of biofilm and surrounding environment plays an important role in determining their morphogenesis, final shape, and internal structure. [100] Especially, experimental observations and time-resolved 3D reconstruction of growing *Vibrio cholerae* biofilm show that the intrinsic anisotropic shape of cells initially causes elongated growth of small clusters, and subsequent cell division along its long axis (Figure 7e). [100] In a soft environment, the biofilms eventually assume a spherical shape with random cellular organization. In a stiff environment (e.g., agarose gel), however, growth-induced stresses across the biofilm interface result in the oblate spheroidal shape of biofilm in which the cells are aligned tangentially at the interface and radially around two poles (Figure 7e). This configuration is consistent with the bipolar organization of

LC droplet (Figure 2e) that has a point defect of $m = +1$ at each pole. [29, 100] These findings increase understanding of how bacterial communities develop under mechanical constraints, and thus provide resources that can be used to control the growth of biofilm in three-dimensional environments.

In addition, Zhou *et al.* introduce a new class of active matter, living liquid crystals that are composed of swimming bacteria of *Bacillus subtilis* in the liquid crystalline aqueous solution of DSCG. [103] They find that bacterial activity can have a profound effect on the LC media. As shown in Figure 7f-h, bacterial motions generate persistent rearrangement of not only bacteria, but also of DSCG and thereby cause spatiotemporal patterns with continuous nucleation and annihilation of topological defects of $m = \pm 1/2$. As such, LC medium provides optically accessible information on microscopic bacterial behavior that will be of interest for further investigation. In the following section, we will explore in more detail how bacterial behaviors are mediated in LC media.

3. Motile bacteria in LCs

In this section, we discuss motile bacteria in a non-equilibrium system. Recent advances in active-matter and active-LCs are represented by rod-shaped motile bacteria that have sizes in the range of nanometer-sized DNAs to microscale CNCs. Recent research has extended studies on bacterial motion at interfaces of isotropic liquids [99, 104] to develop an understanding of the behavior and dynamics of bacteria at the interfaces of, and within, anisotropic complex fluids. [105, 106] These studies provide new insights into dynamic phenomena resulting from the coupling between bacteria-induced flow and long-range molecular ordering of LCs. [103, 107-112] Examples include (i) an activity-triggered transition from a non-flowing uniform state into a flowing periodic pattern of LCs and its evolution into a turbulent array of topological defects (Figure 7f-h), [103] (ii) trajectories of bacterial motion guided by predesigned profiles of LC director (Figure 8, 9), [110, 113, 114] (iii) local melting of LC caused by shear stress from bacterial motion, [103] and (iv) cargo transport by controlled motion of bacteria or motion-induced flows (Figure 9). [113, 114]

Specifically, Mushenheim *et al*. demonstrate motion of bacteria dispersed in LLCs to be guided by the director profile (Figure 8a). [107] Most notably, the anisotropic elasticity of LCs orients the longitudinal axis of rod-shaped bacteria and directs their motion parallel to **n**

to minimize elastic distortion (and thus the elastic free energy) of LCs (Figure 8a). [107, 111] This biased motion is observed to be lost after the phase transition into an isotropic phase (Figure 8b). Likewise, bacterial motions are observed to be guided along the bend and splay distortions of **n** in the DSCG film with a hybrid surface anchoring (planar and homeotropic surface anchoring at bottom and top substrates, respectively; Figure 8c). [109] Vertically-oriented bacteria at the top substrate (i in Figure 8c, d) swim down to the bottom substrate by following **n** profile (ii and iii in Figure 8c, d). These results demonstrate that the overall motion of bacteria can be controlled by elastic strain stored in the LC medium.

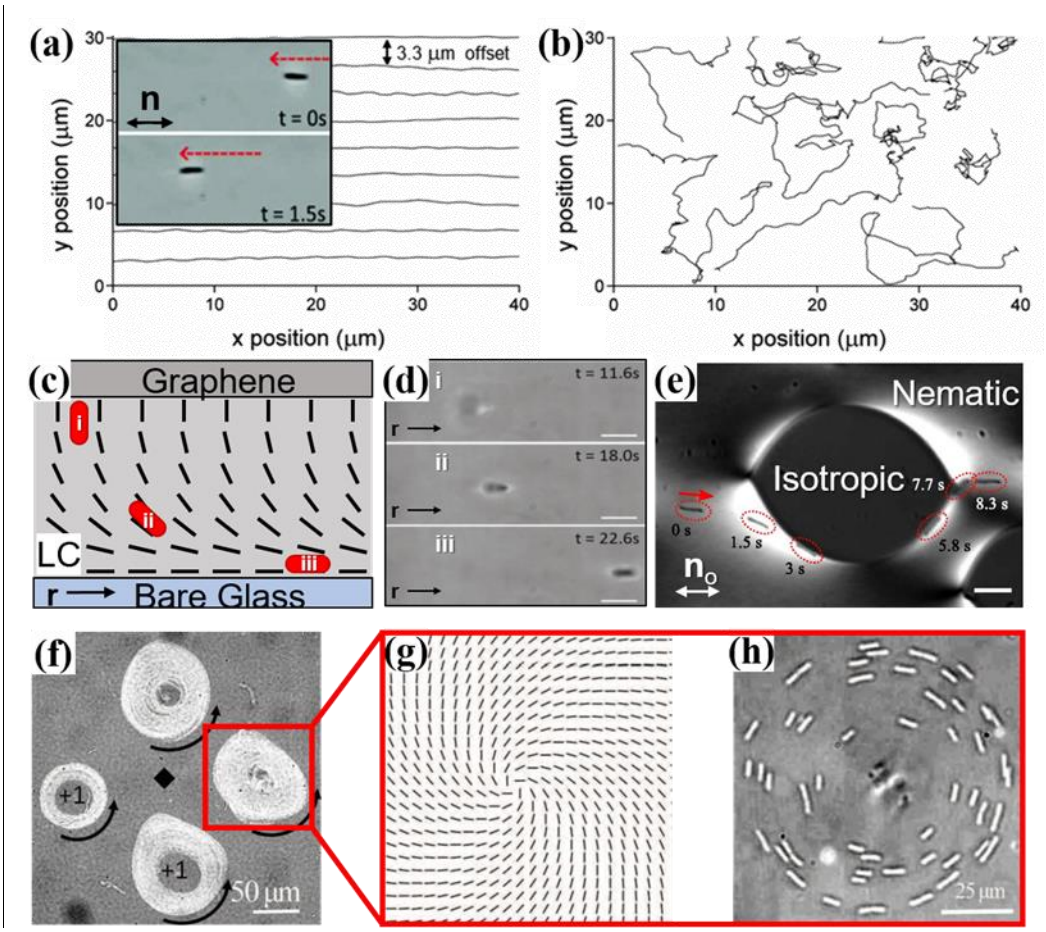

Figure 8. (a, b) Trajectories of swimming motion of *Proteus mirabilis* in (a) a nematic phase (T = 25 °C, **n** || x-axis) and (b) an isotropic phase (T = 42 °C) of DSCG film. Insets in (a) are sequential micrographs of *P. mirabilis* swimming along **n**. (c) Schematic illustration (side view) and (d) corresponding sequential micrographs (top view) for the guided motion of *P. mirabilis* in the DSCG film with hybrid surface anchoring. Black dashed lines and red ellipsoids indicate **n** of DSCG and bacteria, respectively. **r** is the orientation of overall **n** projected onto the substrate. Scale bars, 5 μm. (e) Trajectory of a single bacterium around an isotropic tactoid of DSCG. Scale bars, 5 μm. (f) Superimposed micrographs for the motion of

bacteria guided by (g) prepatterned director profile of DSCG. (h) Corresponding micrograph for the circular motion of bacteria swarm around the defect core of $m = +1$. (a, b) Reproduced with permission. [107] Copyright 2014, Royal Society of Chemistry. (c, d) Reproduced under the terms of the CC-BY-NC Creative Commons Attribution 3.0 International license (https://creativecommons.org/licenses/by-nc/3.0/). [109] Copyright 2015, The Authors, published by Royal Society of Chemistry. (e) Reproduced under the terms of the CC-BY Creative Commons Attribution 4.0 International license (https://creativecommons.org/licenses/by/4.0/). [103] Copyright 2014, The Authors, published by PNAS. (f-h) Reproduced with permission. [110] Copyright 2016, American Association for the Advancement of Science.

Behavior of individual bacteria is also investigated at a biphasic region of LLCs, in which isotropic and nematic phases coexist (Figure 8e). Far away from the isotropic island (dark region in Figure 8e), also known as a negative tactoid (isotropic island in nematic), [22] a bacterium is swimming along the overall director $\mathbf{n_0}$. [103] Near the tactoid, however, the trajectory deviates from $\mathbf{n_0}$ and follows the local distorted director. After colliding with the isotropic-nematic interface, the bacterium follows the curvature of the tactoid and finally escapes at the cusp of tactoids where a topological defect is located. At the biphasic region of LLCs, various types of negative and positive (nematic island in isotropic) tactoids with different set of topological defects exist. The type, size, density, and morphogenesis of these tactoids (including formation and annihilation) can be controlled by simply changing temperature and the rate of temperature change, [22] so these results hint at the possibility of real-time control of bacterial trajectories.

A polymer alignment layer can be used to prepattern the director profile of DSCG, and thus command the motion of bacteria on demand. For example, by photopolymerization of the mixture of nematic LC, monomer, and photoinitiator, a film of LC polymer is obtained as alignment layers of DSCG. [115, 116] **n** of DSCG on the layers is aligned parallel to the predesigned director profile of nematic LCs in the mixture before polymerization (Figure 8f, g). [110, 117, 118] Because the various patterns of director profile are available via this method, the bacterial motion can be precisely programmable. [110] This ability has numerous applications in a variety of fields. For instance, a circular pattern can be used to trap bacteria, because the programmed director profile enforces bacteria to swim circularly around the center of pattern (Figure 8f-h).

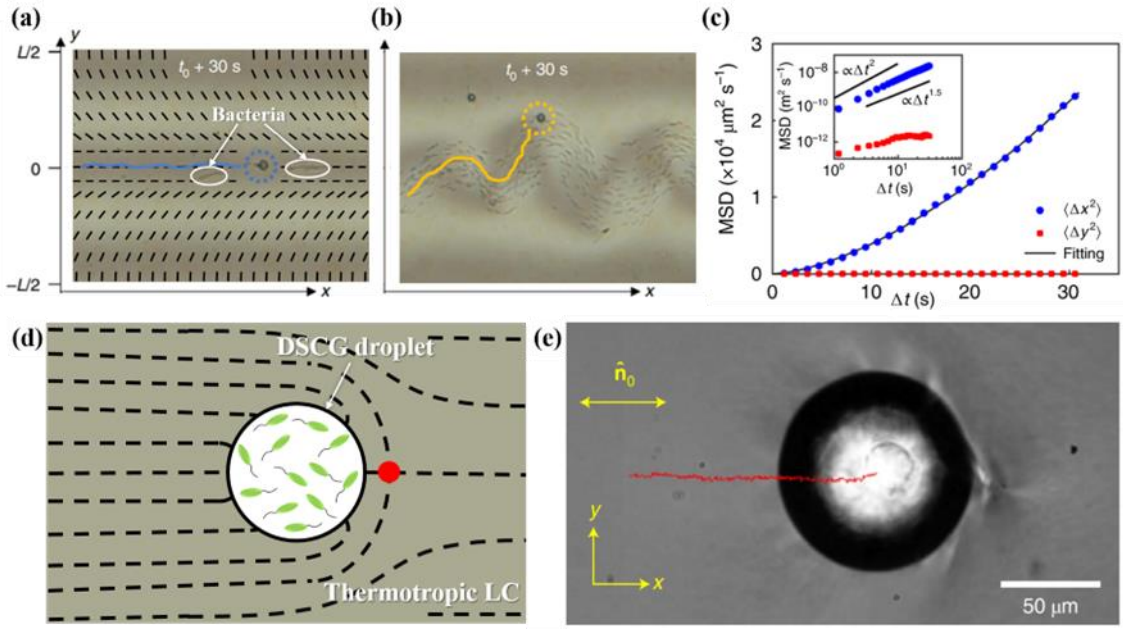

Figure 9. (a, b**)** Microcargo transport by bacterial flow jets induced by the splay-bend director profile of LCs (dashed lines in a) at (a) low and (b) high concentration of bacteria. Blue and yellow lines indicate the trajectories of colloids. (c) Mean squared displacement of the colloids transported by bacterial jets in (a). (d) Schematic illustration of self-propelled droplet of DSCG containing motile bacteria (green ellipsoids with tails) in an inactive medium of thermotropic LC. Black dashed lines and red dot indicate **n** of thermotropic LCs and defect core (hyperbolic hedgehog), respectively. (e) Corresponding micrograph and trajectory (red line) of the self-propelled DSCG droplet along $\mathbf{n_0}$ of LC medium. (a-c) Reproduced with permission. [113] Copyright 2020, Springer Nature. (d, e) Reproduced with permission. [114] Copyright 2020, Springer Nature.

Controlled motion of bacteria by LCs is recently utilized for cargo transport. Turiv *et al.* find splay-bend director profiles of LCs (dashed lines in Figure 9a) induce the bacterial motion that tends to be expelled from the bend regions, but to condense into the splay regions to form polar jets (blue line in Figure 9a). [113] Interestingly, at high concentration of bacteria, the linear bacterial jets are observed to be undulated (Figure 9b). [113, 119, 120] However, the undulations increase elastic and interfacial energy of LCs and thereby suppress growth of the undulating wave beyond the bend regions, which is not possible in isotropic

media. [121-123] Furthermore, both unidirectional and undulating jets can be used to transport colloidal particles along the path of bacteria (Figure 9a-c). [113]

In addition, a new design rule for self-propelled particles is proposed by using DSCG droplets that contain motile bacteria (Figure 9d, e). [114] Specifically, a few mM of surfactants are doped into the DSCG droplet to cause homeotropic surface anchoring of surrounding LCs at the droplet interface. When the droplet is placed in the media of thermotropic LCs with unidirectional alignment of $\mathbf{n_0}$, an asymmetric director structure (black dashed lines in Figure 9d) with a topological defect of $m = +1$ (hyperbolic hedgehog, red dot in Figure 9d) develops around the droplet. Because internal bacterial flows within the DSCG droplet cause reorientation of surrounding LCs, the droplets acquire self-propulsive ability. Furthermore, the elastic strain and asymmetric director profile of surrounding LCs result in linear motion of the droplet along $\mathbf{n_0}$ toward the hyperbolic hedgehog (Figure 9e). [114, 124-126] Such transport systems induced by bacterial activity coupled with LCs will find applications in a variety of fields, including drug-delivery systems.

4. Design of Bio-Sensors with LCs

The COVID-19 pandemic emphasizes the importance on rapid detection of viruses with high sensitivity and selectivity. Especially, as high contagiousness and continuous mutation of COVID-19 cause global health force shortage, development of simple diagnosis techniques that can be used even by untrained people have been demanded. To this end, LCs can be a promising platform to satisfy these demands, due to extraordinary sensitivity and amplification ability that can sense various stimuli, including molecular and nano-scale cues, and convert them to macroscopic optical outputs. [6, 8, 9] We note that remarkable stimuli-sensitivity of LCs has been experimentally demonstrated by previous works, including detection of endotoxin to concentration as low as 1 pg/ml [29] and extremely weak shear stress caused by motile bacteria. [7]

The aqueous-LC interface has been most widely used in the design of biosensors due to its unique characteristics: (i) deformable interface, (ii) ready transport of target biomolecules through the aqueous phase, and (iii) free movement of adsorbed biomolecules at the aqueous-LC interface. [5] Figure 10a-d shows the simplest geometry of LC-based biosensors with an aqueous interface. LC films are hosted in micro-wells supported on a

bounding substrate with a homeotropic anchoring (Figure 10c), and immersed under an aqueous solution. Because LCs assume a planar orientation at aqueous interfaces, the LC films initially show birefringent texture between crossed polarizers (Figure 10a). [9-11, 127, 128] When amphiphilic biomolecules (e.g., endotoxin, [29] phospholipid, [11, 127-129] bile acid [130]) are introduced in the overlying aqueous phase, they self-assemble at the aqueous-LC interface and their tails interdigitate between LCs (Figure 10d). As a result, the LCs assume a vertical orientation at the aqueous interface, and this change causes a rapid, macroscopic optical transition to a dark texture (Figure 10b) that reports the presence of the adsorbates. [9-11, 127, 128]

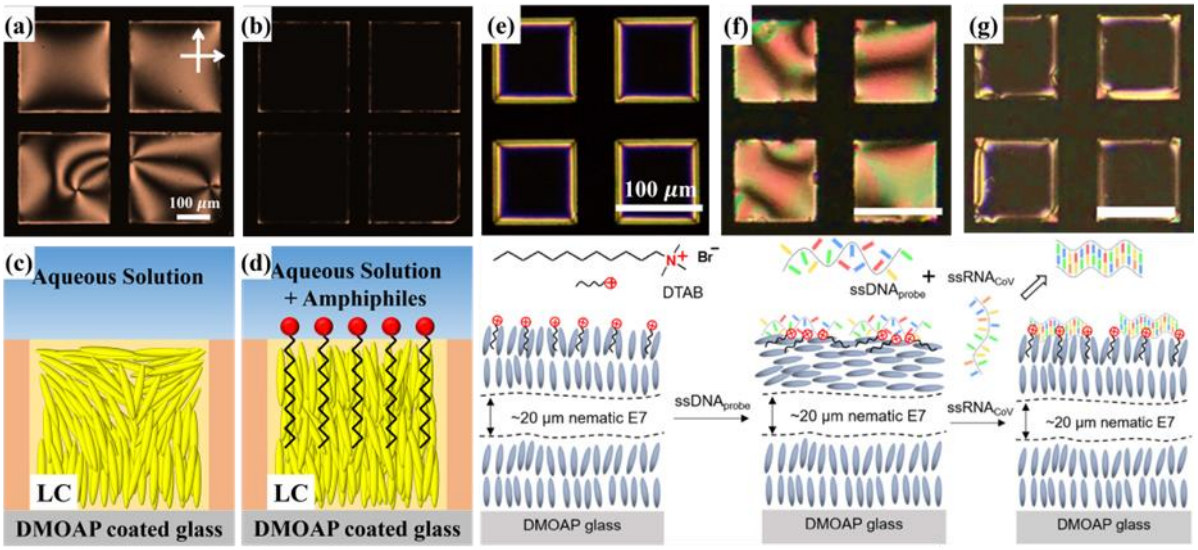

Figure 10. (a, b) Micrographs (top view) and (c, d) schematic illustrations (side view) of LC-based biosensor with an aqueous interface (a, c) before and (b, d) after introduction of amphiphilic biomolecules. (e-g) Design of LC-based virus sensor for SARS-CoV-2. (e) Preparation of homeotropically-aligned LC film immersed under an aqueous solution. DMOAP-treated solid substrate and DTAB-decorated LC interface impose vertical orientation of LCs across the film. (f) Final procedure for the preparation of SARS-CoV-2 sensor. ssDNA of target virus is self-assembled onto the DTAB-decorated LC interface, leading to birefringent signal of LCs. (g) Selective detection of SARS-CoV-2. Injection of ssRNA of target virus selectively interact with the pre-treated ssDNA. Their combination restores the role of DTAB on LCs and thus the vertical orientation, which is signaled by optical transition from birefringent to dark texture. (a-d) Reproduced with permission. [9] Copyright 2018, American Chemical Society. (e-g) Reproduced under the terms of the CC-BY-NC-ND Creative Commons Attribution 4.0 International license

Ribonucleic acid (RNA) and complementary interaction of RNAs have been shown to influence the orientation of LCs at aqueous-LC interfaces. Recent work has exploited the coupling of RNA with LCs to design LC sensors for rapid and selective defection of SARS-CoV-2. [131] First, a homeotropically-aligned LC film is prepared in an aqueous solution (Figure 10e). To this end, bounding substrate of the LC film is coated with dimethyloctadecyl[3-(trimethoxysilyl)propyl]ammonium chloride (DMOAP), and the aqueous-LC interface are decorated with dodecyltrimethylammonium bromide (DTAB). Next, ssDNA of target virus is self-assembled by electrostatic interaction at the DTAB-decorated LC interface. The self-assembly of ssDNA weakens the interaction of DTAB with LCs, so they deviate LCs from the vertical orientation at the aqueous interface, which is reflected by an appearance of birefringent texture (Figure 10f). If single-stranded RNA (ssRNA) of SARS-CoV-2 is introduced, it selectively interacts with pre-treated ssDNA. DNA hybridization between complementary nucleotides reduces the hydrophobic effect of bases. Therefore, the combination of ssDNA and ssRNA restores the efficient packing of DTAB and thus the homeotropic anchoring of LCs at the aqueous-LC interface, leading to the optical transition into dark texture (Figure 10g). The results demonstrate the LC-based biosensor for COVID-19 virus to satisfy the needs for (i) simplicity (no requirement of any complex instrumentation), (ii) rapid and simple diagnosis (instant response of LCs signaled by direct macroscopic optical output), (iii) high sensitivity as a result of the amplification ability of LCs, and (iv) high selectivity by pre-treated ssDNA that only interacts with target ssRNA over a specific number of bases.

The unique characteristics of LCs can also facilitate detection of bacteria (Figure 11). [7] Recent work by Kim *et al.* demonstrates that even the very weak interfacial shear stress induced by bacterial motion at an aqueous-LC interface can overcome the elastic torque of LCs, and thus induce transient reorientation of local **n**, leading to macroscopic optical signal for the arrival of bacteria (Figure 11e). [7] Moreover, the shear-induced reorientation of LCs is demonstrated to manipulate the force balance acting on guest droplets in LCs. By leveraging this, a new class of smart materials has been designed that can not only autonomously sense and optically report the arrival of bacteria, but also trigger the release of

aqueous droplets containing anti-bacterial agents from LCs (Figure 11c) via the modulation of electrostatic attraction (F_{edl}, red arrow in Figure 11a) and elastic repulsion (F_{e1}, blue arrow in Figure 11a) between aqueous-LC and droplet interfaces. The most striking feature of smart LC is its self-regulating ability. For instance, the LCs neither show the optical signal nor release the droplets in the absence of bacteria or in the presence of weakly-motile bacteria (Figure 11b). Furthermore, after the release of anti-bacterial agents kills the motile bacteria (and thus eliminates interfacial shear stress), smart LCs cease both optical reporting and release (Figure 11d). We note that this is the first example of a material that is capable of self-regulated release of chemical agents in response to the motion of living cells.

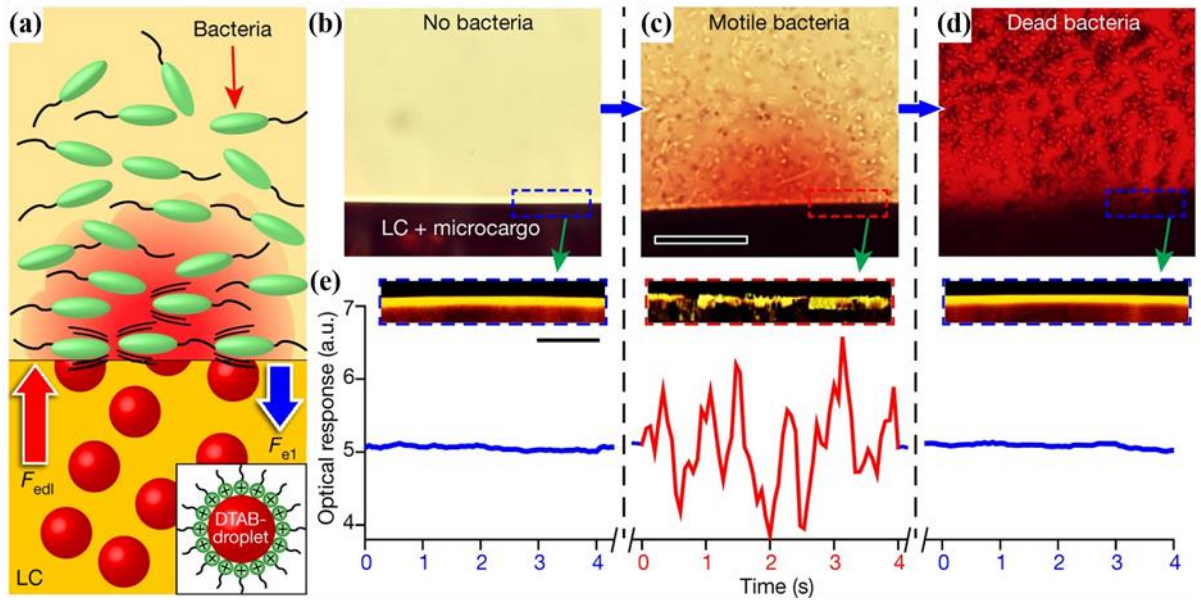

Figure 11. (a) Schematic illustration of self-reporting and self-regulating LCs that optically report the arrival of bacteria and then release the anti-bacterial agents trapped within the LCs. (b-d) Corresponding sequential micrographs (b) before (no bacteria), (c) right after (optical reporting and release of anti-bacterial agents), and (d) two hours (cell death) after the arrival of bacteria. Scale bar, 10 μm. Optical responses and side views (between crossed polars) of the aqueous-LC interface corresponding to (b-d). (a-e) Reproduced with permission. [7] Copyright 2018, Springer Nature.

5. Conclusion

In this review, we describe recent studies including liquid crystalline biomaterials and interactions between biomaterials and LCs. In Section 2, we note LLCs derived from

biomaterials, including DNA, CNCs, and bacteria. Rod-like DNA can form various LC phases including a 'hidden' smectic phase that has only been observed recently, which helps to understand complicated bio-nanostructures. In addition, due to LC behavior of DNAs, their orientational ordering can be precisely programmed by external forces or patterned substrates. Therefore, DNA-based LCs can be utilized as a soft template to align molecular/colloidal guest materials. CNCs spontaneously form left-handed cholesteric LCs due to asymmetric carbons. [48] This helical structure allows cholesteric CNCs to develop quasi-layers, which induce Bragg reflection. Because the cholesteric CNCs can readily tune their chiral pitch (*p*) in response to external stimuli (e.g., relative humidity, mechanical stress), they can freely change the reflection wavelength of light from visible to near-infrared. In addition to this characteristic, CNCs are abundant and renewable, so they have been considered as promising photonic materials that can broaden optical applications without the need to synthesize new materials. However, use of CNCs in industry requires scaling up of production and film size; this is a remaining challenge. Bacteria that are rod-like shape also form LC phases with topological defects when they become a colony. Interpretation of bacteria with LC perspective can improve our understanding of physical behaviors of bacteria such as morphogenesis of cell colony and internal organization of cells in colony.

Studies of bacterial motion in LLC media offer insight into their dynamics in a non-equilibrium system. Section 3 shows in detail that bacterial motion can be manipulated by LC characteristics of surrounding media. Specifically, the elasticity and long-range molecular ordering of LLC media can predesign migration pathways of motile bacteria. In addition, the elastic and interfacial energies of LLCs can generate and control the bacterial flow; such control is not possible in isotropic fluids. The results offer possibility for controlled transport of microcargo by bacteria with LLCs. Especially, the existence of biphasic region in LLCs allows morphogenesis of various types of topological defects and tactoids (nematic domain in isotropic or isotropic domain in nematic), thus providing further design rules to manipulate the dynamics of bacteria. [22] Hence, the studies on the integration of bacteria in LLCs can offer access to deep understanding of bacterial dynamics that will be uses in a variety of bioengineering applications.

In section 4, we describe LC-based biosensors using advantages of an aqueous-LC interface, including deformable interface, ready transport of bio-target, and free movement of adsorbates at the interface. Due to extraordinary stimuli-responsiveness and interactions with

biomaterials, LCs instantly sense the arrival of target stimuli (e.g., bacteria, COVID-19) and reorient their directors, leading to macroscopic optical signal. In addition, the stimuli-triggered reorientation of directors modulates forces acting on the guest materials within LCs, so one can introduce additional functionalities into the LC-based biosensor (e.g., self-regulated release of drug, self-regulated polymerization). [7, 132] Recently, the LC-based sensors have been integrated with metasurface (MS) to overcome challenges in metahologram. The LC-MS system realizes the new class of interactive metahologram that autonomously sense a target stimulus (e.g., electric field, toxic gas, pressure, temperature) and instantaneously change holographic images that was not available in previous systems. [13, 14, 133]

To summarize, the strong interactions between biomaterials and LCs addressed in this review will provide deep understanding of the gap in knowledge in bioscience, and offer general and versatile approach to the rational design of smart systems to satisfy the needs that not only sense target stimuli (including molecular and nanoscopic phenomena) and optically report them, but also transform the environment via self-regulated functions.

Acknowledgements

This work is supported by the Korean National Research Foundation (NRF) grants (NRF-2021R1A2C2095010, NRF-2021R1A4A1030944) funded by the Korean government and the POSCO Science fellowship funded by POSCO TJ Park Foundation. We thank Yeongseon Choi for offering micrographs in Figure 1c.

Reference

[1] P. G. de Gennes, J. Prost, *The Physics of Liquid Crystals*, Clarendon Press, Oxford **1993**.

[2] M. Kleman, O. D. Lavrentovich, *Soft Matter Physics: An Introduction*, Springer, New York **2003**.

[3] P. J. Collings, M. Hird, *Introduction to Liquid Crystals Chemistry and Physics*, CRC Press, London **1997**.

[4] P. J. Collings, *Liquid Crystals: Nature's Delicate Phase of Matter*, Princeton University Press, **2002**.

[5] E. Bukusoglu, M. B. Pantoja, P. C. Mushenheim, X. Wang, N. L. Abbott, *Annu. Rev. Chem. Biomol. Eng.* **2016**, *7*, 163.

[6] Y.-K. Kim, J. Noh, K. Nayani, N. L. Abbott, *Soft Matter* **2019**, *15*, 6913.

[7] Y.-K. Kim, X. Wang, P. Mondkar, E. Bukusoglu, N. L. Abbott, *Nature* **2018**, *557*, 539.

[8] Y.-K. Kim, Y. Huang, M. Tsuei, X. Wang, N. C. Gianneschi, N. L. Abbott, *ChemPhysChem* **2018**, *19*, 2037.

[9] Y.-K. Kim, K. R. Raghupathi, J. S. Pendery, P. Khomein, U. Sridhar, J. J. de Pablo, S. Thayumanavan, N. L. Abbott, *Langmuir* **2018**, *34*, 10092.

[10] H. Ramezani-Dakhel, M. Rahimi, J. Pendery, Y.-K. Kim, S. Thayumanavan, B. Roux, N. L. Abbott, J. J. de Pablo, *ACS Appl. Mater. Interfaces* **2018**, *10*, 37618.

[11] M. Tsuei, M. Shivrayan, Y.-K. Kim, S. Thayumanavan, N. L. Abbott, *J. Am. Chem. Soc.* **2020**, *142*, 6139.

[12] Y. Yang, Y.-K. Kim, X. Wang, M. Tsuei, N. L. Abbott, *ACS Appl. Mater. Interfaces* **2020**, *12*, 42099.

[13] I. Kim, M. A. Ansari, M. Q. Mehmood, W.-S. Kim, J. Jang, M. Zubair, Y.-K. Kim, J. Rho, *Adv. Mater.* **2020**, *32*, 2004664.

[14] I. Kim, W.-S. Kim, K. Kim, M. A. Ansari, M. Q. Mehmood, T. Badloe, Y. Kim, J. Gwak, H. Lee, Y.-K. Kim, J. Rho, *Sci. Adv.* **2021**, *7*, eabe9943.

[15] L. De Sio, J. G. Cuennet, A. E. Vasdekis, D. Psaltis, *Appl. Phys. Lett.* **2010**, *96*, 131112.

[16] Y.-K. Kim, B. Senyuk, O. D. Lavrentovich, *Nat. Commun.* **2012**, *3*, 1133.

[17] X. Wang, Y.-K. Kim, E. Bukusoglu, B. Zhang, D. S. Miller, N. L. Abbott, *Phys. Rev. Lett.* **2016**, *116*, 147801.

[18] A. J. J. Kragt, R. C. G. M. Loonen, D. J. Broer, M. G. Debije, A. P. H. J. Schenning, *J. Polym. Sci.* **2021**, *59*, 1278.

[19] W. Meng, Y. Gao, X. Hu, L. Tan, L. Li, G. Zhou, H. Yang, J. Wang, L. Jiang, *ACS Appl. Mater. Interfaces* **2022**, *14*, 28301.

[20] C. S. Park, K. Iwabata, U. Sridhar, M. Tsuei, K. Singh, Y.-K. Kim, S. Thayumanavan, N. L. Abbott, *ACS Appl. Mater. Interfaces* **2020**, *12*, 7869.

[21] M. Tsuei, H. Sun, Y.-K. Kim, X. Wang, N. C. Gianneschi, N. L. Abbott, *Langmuir* **2022**, *38*, 332.

[22] Y.-K. Kim, S. V. Shiyanovskii, O. D. Lavrentovich, *J. Phys.: Condens. Matter* **2013**, *25*, 404202.

[23] J. Xiang, Y. Li, Q. Li, D. A. Paterson, J. M. D. Storey, C. T. Imrie, O. D. Lavrentovich, *Adv. Mater.* **2015**, *27*, 3014.

[24] J. Xiang, A. Varanytsia, F. Minkowski, D. A. Paterson, J. M. D. Storey, C. T. Imrie, O. D. Lavrentovich, P. Palffy-Muhoray, *Proc. Natl. Acad. Sci. USA* **2016**, *113*, 12925.

[25] Y.-K. Kim, G. Cukrov, F. Vita, E. Scharrer, E. T. Samulski, O. Francescangeli, O. D. Lavrentovich, *Phys. Rev. E* **2016**, *93*, 062701.

[26] R. Mangal, K. Nayani, Y.-K. Kim, E. Bukusoglu, U. M. Córdova-Figueroa, N. L. Abbott, *Langmuir* **2017**, *33*, 10917.

[27] C. W. Shields IV, Y.-K. Kim, K. Han, A. C. Murphy, A. J. Scott, N. L. Abbott, O. D. Velev, *Adv. Intell. Syst.* **2020**, *2*, 1900114.

[28] Y.-K. Kim, B. Senyuk, S.-T. Shin, A. Kohlmeier, G. H. Mehl, O. D. Lavrentovich, *Soft Matter* **2014**, *10*, 500.

[29] I. H. Lin, D. S. Miller, P. J. Bertics, C. J. Murphy, J. J. de Pablo, N. L. Abbott, *Science* **2011**, *332*, 1297.

[30] I. Dierking, A. M. F. Neto, *Crystals* **2020**, *10*, 604.

[31] J. C. Weaver, G. W. Milliron, A. Miserez, K. Evans-Lutterodt, S. Herrera, I. Gallana, W. J. Mershon, B. Swanson, P. Zavattieri, E. DiMasi, D. Kisailus, *Science* **2012**, *336*, 1275.

[32] L. Fernández Del Río, H. Arwin, K. Järrendahl, *Thin Solid Films* **2014**, *571*, 410.

[33] G. Agez, C. Bayon, M. Mitov, *Acta Biomaterialia* **2017**, *48*, 357.

[34] A. Tran, C. E. Boott, M. J. MacLachlan, *Adv. Mater.* **2020**, *32*, 1905876.

[35] K. Nayani, A. A. Evans, S. E. Spagnolie, N. L. Abbott, *Proc. Natl. Acad. Sci. USA* **2020**, *117*, 26083.

[36] F. Livolant, A. Leforestier, *Prog. Polym. Sci.* **1996**, *21*, 1115.

[37] L. Onsager, *Ann. N. Y. Acad. Sci.* **1949**, *51*, 627.

[38] J. Vieillard-Baron, *Mol. Phys.* **1974**, *28*, 809.

[39] A. Stroobants, H. N. W. Lekkerkerker, D. Frenkel, *Phys. Rev. A* **1987**, *36*, 2929.

[40] D. Frenkel, *Liq. Cryst.* **1989**, *5*, 929.

[41] P. Bolhuis, D. Frenkel, *J. Chem. Phys.* **1997**, *106*, 666.

[42] P. J. Hagerman, *Annu. Rev. Biophys. Biophys. Chem.* **1988**, *17*, 265.

[43] R. L. Rill, T. E. Strzelecka, M. W. Davidson, D. H. Van Winkle, *Physica A* **1991**, *176*, 87.

[44] Y. M. Yevdokimov, V. I. Salyanov, S. V. Semenov, S. G. Skuridin, *DNA liquid-crystalline dispersions and nanoconstructions*, CRC Press, Boca Raton **2011**.

[45] C. Tschierske, *Liquid Crystals: Materials Design and Self-Assembly*, Vol. 318, Springer, Berlin **2012**.

[46] B. A. Todd, V. A. Parsegian, A. Shirahata, T. J. Thomas, D. C. Rau, *Biophys. J.* **2008**, *94*, 4775.

[47] Y. M. Yevdokimov, S. G. Skuridin, V. I. Salyanov, S. V. Semenov, E. Kats, *Crystals* **2019**, *9*, 162.

[48] L. Wang, A. M. Urbas, Q. Li, *Adv. Mater.* **2020**, *32*, 1801335.

[49] C. Robinson, *Tetrahedron* **1961**, *13*, 219.

[50] E. Iizuka, *Polym. J.* **1977**, *9*, 173.

[51] T. E. Strzelecka, M. W. Davidson, R. L. Rill, *Nature* **1988**, *331*, 457.

[52] M. De Frutos, A. Leforestier, F. Livolant, *Biophys. Rev. Lett.* **2013**, *9*, 81.

[53] M. Nakata, G. Zanchetta, B. D. Chapman, C. D. Jones, J. O. Cross, R. Pindak, T. Bellini, N. A. Clark, *Science* **2007**, *318*, 1276.

[54] T. P. Fraccia, G. P. Smith, L. Bethge, G. Zanchetta, G. Nava, S. Klussmann, N. A. Clark, T. Bellini, *ACS Nano* **2016**, *10*, 8508.

[55] G. P. Smith, T. P. Fraccia, M. Todisco, G. Zanchetta, C. Zhu, E. Hayden, T. Bellini, N. A. Clark, *Proc. Natl. Acad. Sci. USA* **2018**, *115*, E7658.

[56] C. S. Swenson, H. H. Lackey, E. J. Reece, J. M. Harris, J. M. Heemstra, E. M. Peterson, *RSC Chem. Biol.* **2021**, *2*, 1249.

[57] L. S. Lerman, *Proc. Natl. Acad. Sci. USA* **1971**, *68*, 1886.

[58] J. É. B. Ramos, R. de Vries, J. R. Neto, *J. Phys. Chem. B* **2005**, *109*, 23661.

[59] E. Grelet, M. P. Lettinga, M. Bier, R. van Roij, P. van der Schoot, *J. Phys.: Condens. Matter* **2008**, *20*, 494213.

[60] A. Kuijk, D. V. Byelov, A. V. Petukhov, A. van Blaaderen, A. Imhof, *Faraday Discuss.* **2012**, *159*, 181.

[61] F. Livolant, Y. Bouligand, *J. phys.* **1986**, *47*, 1813.

[62] F. Livolant, A. M. Levelut, J. Doucet, J. P. Benoit, *Nature* **1989**, *339*, 724.

[63] M. Salamonczyk, J. Zhang, G. Portale, C. Zhu, E. Kentzinger, J. T. Gleeson, A. Jakli, C. De Michele, J. K. G. Dhont, S. Sprunt, E. Stiakakis, *Nat. Commun.* **2016**, *7*, 13358.

[64] P. Gyawali, R. Saha, G. P. Smith, M. Salamonczyk, P. Kharel, S. Basu, R. Li, M. Fukuto, J. T. Gleeson, N. A. Clark, A. Jákli, H. Balci, S. Sprunt, *Proc. Natl. Acad. Sci. USA* **2021**, *118*, e2019996118.

[65] E. Pouget, E. Grelet, M. P. Lettinga, *Phys. Rev. E* **2011**, *84*, 041704.

[66] A. Bensimon, A. Simon, A. Chiffaudel, V. Croquette, F. Heslot, D. Bensimon, *Science* **1994**, *265*, 2096.

[67] N. Morii, G. Kido, H. Suzuki, S. Nimori, H. Morii, *Biomacromolecules* **2004**, *5*, 2297.

[68] Y. J. Cha, M.-J. Gim, H. Ahn, T. J. Shin, J. Jeong, D. K. Yoon, *ACS Appl. Mater. Interfaces* **2017**, *9*, 18355.

[69] Y. J. Cha, D. K. Yoon, *Adv. Mater.* **2017**, *29*, 1604247.

[70] Y. J. Cha, S. M. Park, R. You, H. Kim, D. K. Yoon, *Nat. Commun.* **2019**, *10*, 2512.

[71] N. P. Dhakal, J. Jiang, Y. Guo, C. Peng, *Phys. Rev. Appl.* **2020**, *13*, 014026.

[72] I. I. Smalyukh, J. Butler, J. D. Shrout, M. R. Parsek, G. C. L. Wong, *Phys. Rev. E* **2008**, *78*, 030701.

[73] Y. J. Cha, M.-J. Gim, K. Oh, D. K. Yoon, *ACS Appl. Mater. Interfaces* **2015**, *7*, 13627.

[74] B. Zhang, J. Schmidtke, H.-S. Kitzerow, *Adv. Opt. Mater.* **2019**, *7*, 1801766.

[75] X. Xu, P. Winterwerber, D. Ng, Y. Wu, *Top. Curr. Chem.* **2020**, *378*, 31.

[76] C. J. Whitfield, M. Zhang, P. Winterwerber, Y. Wu, D. Y. W. Ng, T. Weil, *Chem. Rev.* **2021**, *121*, 11030.

[77] R. J. Kline, M. D. McGehee, E. N. Kadnikova, J. Liu, J. M. J. Fréchet, M. F. Toney, *Macromolecules* **2005**, *38*, 3312.

[78] M. J. Han, M. McBride, B. Risteen, G. Zhang, B. V. Khau, E. Reichmanis, D. K. Yoon, *Chem. Mater.* **2020**, *32*, 688.

[79] S. Dey, C. Fan, K. V. Gothelf, J. Li, C. Lin, L. Liu, N. Liu, M. A. D. Nijenhuis, B. Saccà, F. C. Simmel, H. Yan, P. Zhan, *Nat. Rev. Methods Primers* **2021**, *1*, 13.

[80] M. Siavashpouri, C. H. Wachauf, M. J. Zakhary, F. Praetorius, H. Dietz, Z. Dogic, *Nat. Mater.* **2017**, *16*, 849.

[81] H. J. Philipp, M. L. Nelson, H. M. Ziifle, *Text. Res. J.* **1947**, *17*, 585.

[82] I. I. Smalyukh, *Adv. Mater.* **2021**, *33*, 2001228.

[83] A. G. Dumanli, H. M. van der Kooij, G. Kamita, E. Reisner, J. J. Baumberg, U. Steiner, S. Vignolini, *ACS Appl. Mater. Interfaces* **2014**, *6*, 12302.

[84] B. Frka-Petesic, G. Guidetti, G. Kamita, S. Vignolini, *Adv. Mater.* **2017**, *29*, 1701469.

[85] R. Xiong, S. Yu, M. J. Smith, J. Zhou, M. Krecker, L. Zhang, D. Nepal, T. J. Bunning, V. V. Tsukruk, *ACS Nano* **2019**, *13*, 9074.

[86] A. G. Dumanli, G. Kamita, J. Landman, H. van der Kooij, B. J. Glover, J. J. Baumberg, U. Steiner, S. Vignolini, *Adv. Opt. Mater.* **2014**, *2*, 646.

[87] Q. Chen, P. Liu, F. Nan, L. Zhou, J. Zhang, *Biomacromolecules* **2014**, *15*, 4343.

[88] K. Yao, Q. Meng, V. Bulone, Q. Zhou, *Adv. Mater.* **2017**, *29*, 1701323.

[89] J. A. De La Cruz, Q. Liu, B. Senyuk, A. W. Frazier, K. Peddireddy, I. I. Smalyukh, *ACS Photonics* **2018**, *5*, 2468.

[90] O. Kose, A. Tran, L. Lewis, W. Y. Hamad, M. J. MacLachlan, *Nat. Commun.* **2019**, *10*, 510.

[91] O. Kose, C. E. Boott, W. Y. Hamad, M. J. MacLachlan, *Macromolecules* **2019**, *52*, 5317.

[92] C. E. Boott, A. Tran, W. Y. Hamad, M. J. MacLachlan, *Angew. Chem. Int. Ed.* **2020**, *59*, 226.

[93] B. E. Droguet, H.-L. Liang, B. Frka-Petesic, R. M. Parker, M. F. L. De Volder, J. J. Baumberg, S. Vignolini, *Nat. Mater.* **2022**, *21*, 352.

[94] K. E. Shopsowitz, H. Qi, W. Y. Hamad, M. J. MacLachlan, *Nature* **2010**, *468*, 422.

[95] K. E. Shopsowitz, W. Y. Hamad, M. J. MacLachlan, *J. Am. Chem. Soc.* **2012**, *134*, 867.

[96] Q. Liu, M. G. Campbell, J. S. Evans, I. I. Smalyukh, *Adv. Mater.* **2014**, *26*, 7178.

[97] P.-X. Wang, W. Y. Hamad, M. J. MacLachlan, *Angew. Chem. Int. Ed.* **2016**, *55*, 12460.

[98] M. Chekini, E. Prince, L. Zhao, H. Mundoor, I. I. Smalyukh, E. Kumacheva, *Adv. Opt. Mater.* **2020**, *8*, 1901911.

[99] M. Rosenberg, *FEMS Microbiol. Lett.* **1984**, *22*, 289.

[100] Q. Zhang, J. Li, J. Nijjer, H. Lu, M. Kothari, R. Alert, T. Cohen, J. Yan, *Proc. Natl. Acad. Sci. USA* **2021**, *118*, e2107107118.

[101] R. C. McKellar, X. Lu, *Modeling Microbial Responses in Food*, CRC press, Boca Raton **2003**.

[102] D. Dell'Arciprete, M. L. Blow, A. T. Brown, F. D. C. Farrell, J. S. Lintuvuori, A. F. McVey, D. Marenduzzo, W. C. K. Poon, *Nat. Commun.* **2018**, *9*, 4190.

[103] S. Zhou, A. Sokolov, O. D. Lavrentovich, I. S. Aranson, *Proc. Natl. Acad. Sci. USA* **2014**, *111*, 1265.

[104] Z. Kang, A. Yeung, J. M. Foght, M. R. Gray, *Colloids Surf. B: Biointerfaces* **2008**, *67*, 59.

[105] O. D. Lavrentovich, *Curr. Opin. Colloid Interface Sci.* **2016**, *21*, 97.

[106] R. Zhang, A. Mozaffari, J. J. de Pablo, *Nat. Rev. Mater.* **2021**, *6*, 437.

[107] P. C. Mushenheim, R. R. Trivedi, H. H. Tuson, D. B. Weibel, N. L. Abbott, *Soft Matter* **2014**, *10*, 88.

[108] P. C. Mushenheim, R. R. Trivedi, D. B. Weibel, N. L. Abbott, *Biophys. J.* **2014**, *107*, 255.

[109] P. C. Mushenheim, R. R. Trivedi, S. S. Roy, M. S. Arnold, D. B. Weibel, N. L. Abbott, *Soft Matter* **2015**, *11*, 6821.

[110] C. Peng, T. Turiv, Y. Guo, Q.-H. Wei, O. D. Lavrentovich, *Science* **2016**, *354*, 882.

[111] S. Zhou, O. Tovkach, D. Golovaty, A. Sokolov, I. S. Aranson, O. D. Lavrentovich, *New J. Phys.* **2017**, *19*, 055006.

[112] H. Chi, M. Potomkin, L. Zhang, L. Berlyand, I. S. Aranson, *Commun. Phys.* **2020**, *3*, 162.

[113] T. Turiv, R. Koizumi, K. Thijssen, M. M. Genkin, H. Yu, C. Peng, Q.-H. Wei, J. M. Yeomans, I. S. Aranson, A. Doostmohammadi, O. D. Lavrentovich, *Nat. Phys.* **2020**, *16*, 481.

[114] M. Rajabi, H. Baza, T. Turiv, O. D. Lavrentovich, *Nat. Phys.* **2021**, *17*, 260.

[115] Y. Guo, M. Jiang, C. Peng, K. Sun, O. Yaroshchuk, O. D. Lavrentovich, Q.-H. Wei, *Adv. Mater.* **2016**, *28*, 2353.

[116] N. P. Dhakal, J. Jiang, Y. Guo, C. Peng, *ACS Appl. Mater. Interfaces* **2020**, *12*, 13680.

[117] Y. Guo, H. Shahsavan, Z. S. Davidson, M. Sitti, *ACS Appl. Mater. Interfaces* **2019**, *11*, 36110.

[118] Y. Guo, M. Jiang, S. Afghah, C. Peng, R. L. B. Selinger, O. D. Lavrentovich, Q.-H. Wei, *Adv. Opt. Mater.* **2021**, *9*, 2100181.

[119] M. M. Genkin, A. Sokolov, O. D. Lavrentovich, I. S. Aranson, *Phys. Rev. X* **2017**, *7*, 011029.

[120] M. M. Genkin, A. Sokolov, I. S. Aranson, *New J. Phys.* **2018**, *20*, 043027.

[121] D. Saintillan, M. J. Shelley, *Phys. Rev. Lett.* **2008**, *100*, 178103.

[122] A. Be'er, G. Ariel, *Mov. Ecol.* **2019**, *7*, 9.

[123] I. S. Aranson, *Rep. Prog. Phys.* **2022**, *85*, 076601.

[124] O. V. Kuksenok, R. W. Ruhwandl, S. V. Shiyanovskii, E. M. Terentjev, *Phys. Rev. E* **1996**, *54*, 5198.

[125] P. Poulin, H. Stark, T. C. Lubensky, D. A. Weitz, *Science* **1997**, *275*, 1770.

[126] Y. Gu, N. L. Abbott, *Phys. Rev. Lett.* **2000**, *85*, 4719.

[127] J. M. Brake, M. K. Daschner, Y.-Y. Luk, N. L. Abbott, *Science* **2003**, *302*, 2094.

[128] J. M. Brake, N. L. Abbott, *Langmuir* **2007**, *23*, 8497.

[129] I. Pani, F. N. K. M., M. Sharma, S. K. Pal, *Nano Letters* **2021**, *21*, 4546.

[130] B. Gollapelli, A. K. Tatipamula, S. Dewanjee, R. S. Pathinti, J. Vallamkondu, *J. Mater. Chem. C* **2021**, *9*, 13991.

[131] Y. Xu, A. M. Rather, S. Song, J.-C. Fang, R. L. Dupont, U. I. Kara, Y. Chang, J. A. Paulson, R. Qin, X. Bao, X. Wang, *Cell Reports Phys. Sci.* **2020**, *1*, 100276.

[132] X. Wang, H. Sun, Y.-K. Kim, D. B. Wright, M. Tsuei, N. C. Gianneschi, N. L. Abbott, *Adv. Mater.* **2022**, *34*, 2106535.

[133] T. Badloe, J. Kim, I. Kim, W.-S. Kim, W. S. Kim, Y.-K. Kim, J. Rho, *Light Sci. Appl.* **2022**, *11*, 118.

Biographies

Young-Ki Kim (ykkim@postech.ac.kr)
Assistant Professor
Department of Chemical Engineering
Pohang University of Science and Technology (POSTECH), Korea

Biography

Young-Ki Kim is currently an Assistant Professor in Dept. Chemical Engineering, POSTECH, Korea. He received PhD (2015) in Chemical Physics from Liquid Crystal

Institute, Kent State University (Advisor: Prof. Oleg Lavrentovich). He then had worked as a postdoctoral associate in the laboratory of Prof. Nicholas Abbott in the Department of Chemical Engineering at University of Wisconsin-Madison (2015–2018) and Cornell University (2018–2019). His research focuses on the design of functional materials using liquid crystals. Prof. Kim has published 46 papers in peer-reviewed journal including Nature and Science, and received honorable awards including POSCO Science Fellowship, WARF Invention Grant.

Won-Sik Kim (oneto1218@postech.ac.kr)
Ph.D. Student
Department of Chemical Engineering
Pohang University of Science and Technology (POSTECH), Korea

Biography

Won-Sik Kim is currently a Ph.D. student in the Department of Chemical Engineering, POSTECH, Korea. He received B.S. (2020) in Chemical Engineering from POSTECH. He then has worked as a Ph.D. student in Smart Soft Matter laboratory of Prof. Young-Ki Kim in the Department of Chemical Engineering, POSTECH (2020-). He focuses on research of the design of informative sensors based on liquid crystals and orientation control of 2D materials. He has published 3 papers as a co-author in journals including Advanced Materials, Science Advances, and Light: Science & Applications and received an honorable award on leadership field of POSTECHIAN Fellowship.

Jun-Hyung Im (jhim0116@postech.ac.kr)
Ph.D. Student
Department of Chemical Engineering
Pohang University of Science and Technology (POSTECH), Korea

Biography

Jun-Hyung Im is currently a Ph.D. student in the Department of Chemical Engineering, POSTECH, Korea. He received B.S. with Summa Cum Laude in the Department of Organic and Nano Engineering from Hanyang University, Korea in 2020. Since 2020, he has worked as a Ph.D. student in Smart Soft Matter laboratory of Prof. Young-Ki Kim in the Department of Chemical Engineering at POSTECH. He received honorable 1st POSTECHIAN Fellowship in 2021. His research mainly focuses on molecular and colloidal self-assembly mediated by liquid crystals.

Hyein Kim (hyeinkim@postech.ac.kr)
Ph.D. Student
Department of Chemical Engineering
Pohang University of Science and Technology (POSTECH), Korea

Biography

Hyein Kim is currently a Ph.D. student in the Department of Chemical Engineering, POSTECH, Korea. She received B.S. (2017) in Chemistry from Dong-A University and M.S. (2019) in Chemical Materials from Pusan National University (Advisor: Prof. Sung-Ho Jin). She has worked as a Ph.D. Student in Smart Soft Matter laboratory of Prof. Young-Ki Kim in the Department of Chemical Engineering, POSTECH (2020-). Her research focuses on the design of drug delivery, synthesis systems and chemical sensors based on liquid crystals. She received a Best Poster Paper Award at International Meeting on Information Display (2021).

Jin-Kang Choi (choijk98@postech.ac.kr)
Ph.D. Student
Department of Chemical Engineering
Pohang University of Science and Technology (POSTECH), Korea

Biography

Jin-Kang Choi is currently a Ph.D. student in the Department of Chemical Engineering, POSTECH, Korea. He received B.S. (2021) in Chemical Engineering from POSTECH. He then has worked as a Ph.D. student in Smart Soft Matter laboratory of Prof. Young-Ki Kim in the Department of Chemical Engineering at POSTECH (2021–). His research focuses on the design of stimuli-responsive materials using liquid crystals. He received honorable awards including POSTECHIAN Fellowship.

Yena Choi (ynchoi@postech.ac.kr)
Ph.D. Student
Department of Chemical Engineering
Pohang University of Science and Technology (POSTECH), Korea

Biography

Yena Choi is currently a Ph.D. student in the Department of Chemical Engineering, POSTECH, Korea. She received B.S. (2021) in Chemical Engineering from POSTECH. She then has worked as a Ph.D. student in Smart Soft Matter laboratory of Prof. Young-Ki Kim in the Department of Chemical Engineering at POSTECH (2021–). Her research focuses on the design of smart biomaterials using stimuli-responsive liquid crystals. She received honorable awards including Best Undergraduate Researcher Award.

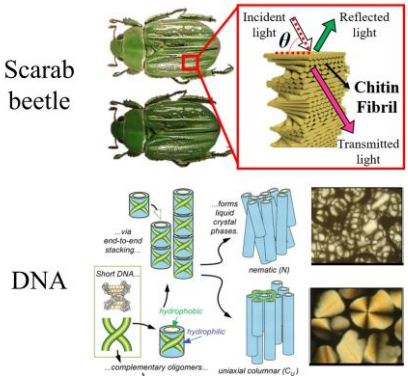

Biomaterials have been extensively explored to understand living organisms and obtain scientific inspiration. However, many aspects are not still fully understood. Because liquid crystalline phases are ubiquitous, therefore, a wide range of research have made attempts to approach unresolved issues with the concept of liquid crystals (LCs). This review presents these studies addressing the interactive correlation between biomaterials and LCs.